Oxidative capacity of the Mexico City atmosphere? Part 2: A ROx radical cycling perspective

P. M. Sheehy, R. Volkamer, L. T. Molina, M. J. Molina

Atmos. Chem. Phys. Discuss., 8, 5359–5412, 2008
www.atmos-chem-phys-discuss.net/8/5359/2008/

Atmospheric Chemistry and Physics Discussions

Oxidative capacity of the Mexico City atmosphere – Part 2: A RO_x radical cycling perspective

P. M. Sheehy[1,2], **R. Volkamer**[1,3,4], **L. T. Molina**[1,2], **and M. J. Molina**[1,3]

[1]Massachusetts Institute of Technology, Cambridge, MA, USA
[2]Molina Center for Energy and the Environment, La Jolla, CA, USA
[3]University of California at San Diego, La Jolla, CA, USA
[4]University of Colorado at Boulder and CIRES, Boulder, CO, USA

Received: 20 December 2007 – Accepted: 16 January 2008 – Published: 17 March 2008

Correspondence to: P. Sheehy (sheehy@alum.mit.edu)

Published by Copernicus Publications on behalf of the European Geosciences Union.

Abstract

A box model using measurements from the Mexico City Metropolitan Area study in the spring of 2003 (MCMA-2003) is presented to study RO_x (RO_x=OH+HO_2+RO_2+RO) radical cycling in the troposphere. Model simulations were performed with the Master Chemical Mechanism (MCMv3.1) constrained with 10 min averaged measurements of major radical sources (i.e., HCHO, HONO, O_3, CHOCHO, etc.), radical sink precursors (i.e., NO, NO_2, SO_2, CO, and 102 volatile organic compounds VOC), meteorological parameters (temperature, pressure, water vapor concentration, dilution), and photolysis frequencies.

Modeled HO_x concentrations compare favorably with measured concentrations for most of the day; however, the model under-predicts the concentrations of radicals in the early morning. This "missing reactivity" is highest during peak photochemical activity, and is least visible in a direct comparison of HO_x radical concentrations. The true uncertainty due to "missing reactivity" is apparent in parameters like chain length, and ozone production ($P(O_3)$). For example, the integral amount of ozone produced could be under-predicted by a factor of two. Our analysis highlights that apart from uncertainties in emissions, and meteorology, there is an additional major chemical uncertainty in current models.

1 Introduction

Implementing robust air pollution control strategies as part of effective air quality management requires a detailed understanding of the oxidative capacity of the atmosphere: The oxidation of volatile organic compounds (VOC) by the hydroxyl radical (OH) initiates radical cycling via HO_x (=OH+HO_2) and NO_x (=NO+NO_2) chemistry in the troposphere that drives a variety of chemical processes, including ozone formation and secondary organic aerosol (SOA) formation. In an urban area, the complexity of the tropospheric chemistry is increased by anthropogenic forcing; as such, sophisticated

ACPD

8, 5359–5412, 2008

chemical models are needed to formulate effective strategies.

The oxidation of VOC generates organic peroxyl radicals, RO_2, which can react with nitric oxide, NO,NO_3, and other RO_2 to form the analog alkoxy radical, RO, and nitrogen dioxide, NO_2. The alkoxy radical reacts in the presence of oxygen to generate the hydroperoxyl radical, HO_2, which will readily react with nitric oxide (NO) to generate recycled OH and nitrogen dioxide (NO_2). The conversion of NO to NO_2 via RO_x cycling in the troposphere is key to the understanding of ozone formation. Studying the processes of these radicals is essential to understanding the general oxidative capacity of the atmosphere.

Radical initiation – the breakdown of a closed shell species yielding a new radical – plays an important role in tropospheric chemistry, as it kick starts the processes that form secondary pollutants; however, radical cycling – the amplification of new radicals in the HO_x-NO_x cycle-dominates in polluted atmospheres i.e., Mexico City Metropolitan Area (MCMA), with propagating reaction rates up to an order of magnitude greater than radical source terms. In a companion paper Volkamer et al. (2007) quantify new radical production ($P(HO_x)$) in the MCMA and on average, 20% of radical production is attributable to the breakdown of closed shell species, while 80% is due to radical cycling. As such, it is important that we understand radical cycling (and recycling), in addition to radical sources.

The behavior of OH and HO_2 under urban tropospheric conditions has only recently been studied. Direct detection of the species is difficult because they are both highly reactive and are present at low concentrations. Although an increasing number of studies combine OH and HO_2 measurements and modeling, only a few field campaigns included HO_x measurements in a polluted urban or semi-urban atmosphere: Measurements of HO_x in an urban atmosphere have been made in London (Abram et al., 2000) and Birmingham UK (Heard et al., 2004); Los Angeles, CA (George et al., 1999); Nashville, TN (Martinez et al., 2003); Houston, TX (Martinez et al., 2002); New York, NY(Ren et al., 2003); near Berlin, Germany (Platt et al., 2002) [1]; at Birmingham

[1]This refers to a semi-rural/urban site near Berlin, Germany. It is important to note that the

near London (Emmerson et al., 2007); and more recently in Mexico City (Shirley et al., 2006). The study described here is characterized by a very polluted airmass in the MCMA with elevated levels of NO_x (>10 ppb).

Measurements during the Los Angeles Free Radical Experiment (LAFRE) were conducted in Claremont, California, 55 km downwind from downtown Los Angeles in September 1993. George et al. (1999) used their own numerical integration program, PAMOL, and a chemical reaction mechanism, CAL (Lurmann et al., 1987), to model HO_x chemistry. They were able to constrain their mechanism with measured values for HO_x, NO_x, O_3, peroxyacetyl nitrate (PAN), H_2O_2, HONO, HNO_3, 100+ VOC, and 9 carbonyl species. The CAL mechanism lumps hydrocarbons according to their reactivity into about a half dozen different surrogate species. The authors noted good agreement between measured and modeled OH measurements, although midday OH was high. Using measured HO_2 as a constraint, they note no differences within systematic uncertainties between calculated and measured concentrations. The authors did not have similar success reproducing HO_2 concentrations, attributed to: incomplete HO_2/RO_2 chemistry, and under-prediction of dicarbonyl photolysis and/or radical sources from reactions between alkenes and ozone.

As part of the $PM_{2.5}$ Technology Assessment Characterization Study in New York (PMTACS-NY), measurements were made at Queens College in the summer of 2001 in a polluted urban environment. Ren et al. (2003) used the Regional Atmospheric Chemistry Mechanism (RACM) (Stockwell et al., 1997), constrained for O_3, NO, NO_2, CO, SO_2, CH_4, HONO, HNO_3, HCHO, and categorized VOC. Generally, they capture the characteristics of HO_x chemistry with their model; however, the model under-predicts HO_2 concentrations at high levels of NO (>50 ppb) occurring in the early morning. They also were unable to reproduce the nighttime levels of OH, as their calculated values were significantly lower than the observed values.

Shirley et al. (2006), also part of the MCMA-2003 campaign, used the same RACM

highest levels of observed NO were limited to a few ppb_v and that there were strong biogenic influences.

model employed by Ren et al. (2003) to investigate HO_x formation. The model was constrained for measured values of O_3, NO, NO_2, CO, SO_2, categorized VOC, water vapor, temperature, pressure, and photolysis frequencies. The results were similar to the analogous calculations by Ren et al. (2003) for New York City: the model produces too little HO_x during the night and morning rush hour and too much during midday, but in general, predicted HO_x within measured and modeled uncertainties.

In the Southern Oxidants Study (SOS) measurements were conducted just 8 km northeast of downtown Nashville, Tennessee in the summer of 1999. The city is surrounded by deciduous forests and pastures, yielding an air mass of anthropogenic and biogenic VOC emissions. Martinez et al. (2003) also employed RACM with measurement constraints for a variety of species, including NO_x, NO_y, HCHO, PAN, and 70+ VOC. Again, the RACM-based model was capable of reproducing the general characteristics of HO_x chemistry; however, at high NO concentrations (a few ppb) they were unable to model the increased HO_2 concentration. The increase in HO_2 meant that ozone production did not decrease at higher concentrations of NO. The authors note an imbalance in the OH budget in their model (i.e. the model is not in steady-state), with additional OH sources required to balance the OH sinks.

In the BERLIner OZone experiment (BERLIOZ), measurements were made at a semi-rural site some 50 km northwest of Berlin, Germany in the summer of 1998. Platt et al. (2002) employed the Master Chemical Mechanism (MCM) (Jenkin et al., 1997), a near-explicit mechanism developed at the University of Leeds, to calculate OH, HO_2 and RO_2 radical concentrations with constraints from measured compounds, including NO_x, O_3, PAN, HCHO, and 71 hydrocarbons. Their model yielded a good qualitative description of the measured diurnal profiles of OH, HO_2 and RO_2. Both the HO_2 and RO_2 concentrations were quantitatively well described by the model. They had problems reproducing OH levels at low levels of NO_x, which they attributed to an incomplete set of VOC mechanisms.

During the Tropospheric ORganic CHemistry experiment (TORCH), measurements were made at Essex, a site 25 miles north east of London during summer of 2003.

The OH and HO_2 radicals were measured via LIF-FAGE technique, and $\Sigma(HO_2+RO_2)$ was measured by a chemical amplification technique. Similar to the work here, Emmerson et al. (2007) used MCMv3.1 to calculate RO_x radical concentrations and radical flux rates for initiation, propagation, and termination pathways. Their model was constrained for 39 VOC species that were directly measured, another 74 VOC by scaling to an emissions scenario suitable for polluted conditions in the United Kingdom, NO_x, O_3, CO, PAN, HCHO, J-values, temperature, and water vapor concentration. Emmerson et al. (2007) also introduced a detailed parameterization to account for heterogeneous loss of HO_2 radicals onto aerosols. In general, they observed good agreement between measured and modeled OH on a daily basis, with a notable over-prediction of OH between 11:00–16:00 (local time) on a diurnal average. Good agreement between measured and modeled HO_2 is also observed on a daily basis, with a notable under-prediction between 06:00–08:30 (local time). Despite this brief under-prediction, they note that the degree of model agreement with HO_2 measurements they report is the best reported under similar conditions (NO<10 ppb).

The focus of this work is similar to that of Emmerson et al. (2007), and includes comparisons between predicted and measured values of OH and HO_2 to RO_x, and a detailed analysis of the impact of radical cycling on the oxidative capacity of the urban troposphere. Our work differs in that we are dealing with extraordinarily high NO_x concentrations and VOC loadings, and explore the effects of these unique characteristics of the airmass on radical initiation (Volkamer et al., 2007) and the amplification of these new radicals. The extensive amount of data collected during the MCMA-2003 campaign (Molina et al., 2007) and recent improvements to the MCM (Bloss et al., 2005a,b) afford a unique opportunity to explore a variety of questions related to RO_x chemistry. In general, predicted HO_x radical concentrations are lower than measured concentrations, and defined here as "missing reactivity". This "missing reactivity" is discussed in greater detail below, and leads to a comprehensive analysis of the mechanism with regard to RO_x cycling. Model scenarios are varied with regard to HO_x to elucidate the effects of "missing reactivity" on VOC oxidation and photochemical ozone

production in the MCMA.

2 The mechanism and the model

The work presented here was performed using the latest version of the Master Chemical Mechanism (MCMv3.1) (Bloss et al., 2005a,b). This version of the MCM includes the degradation kinetics and oxidation schemes of 135 VOC, based on mechanisms described by Jenkin et al. (1997) and Saunders et al. (2003). The updated version includes an improved understanding of aromatic schemes using results from recent laboratory studies (e.g., Olariu et al., 2000; Olariu, 2001; Volkamer et al., 2001; Bethel et al., 2001; Martin et al., 2002; Volkamer et al., 2002). The MCMv3.1 is ideal for a range of NO_x and VOC emission categories because it is a near-explicit mechanism that treats individual reaction pathways rather than lumping them by reactivity. The near-explicit code enables the user to account for individual reactive pathways, which is ideally suited to study RO_x radical cycling. We used the FACSIMILE (Curtis and Sweetenham, 1987) software package as our numerical integrator for the box model.

The model calculations were performed on a 24-h basis, and were initialized every 10-min with the constrained input parameters listed below. The model is constrained for the following major species, including measurement uncertainties: NO (±15%), NO_2 (±20%), HONO (±10%), O_3 (±15%), SO_2 (±20%), and CO (±15%). The model is also constrained for 100 VOC (see Table 1, see below for methodologies and measurement uncertainties), temperature, pressure, water vapor concentration, J-values, and dilution in both the horizontal and vertical fields. Photolysis frequencies were measured by spectroradiometry, and the dilution parameter used is described in detail in a companion paper (Volkamer et al., 2007).

The following modeling scenarios, in terms of constraints, were used to study HO_x chemistry in the MCMA, including estimated model uncertainties for each case:

– HO_x-unconstrained: Only the parameters described above are used to constrain

the mechanism (e.g. VOC, inorganics, etc.). In this case, we report modeled uncertainties for OH and HO_2 of ±55% and ±70%, respectively.

– OH-constrained: A median diurnal profile of OH is used to constrain the mechanism, in addition to the parameters described above. In this case, we estimate an uncertainty of ±60% for HO_2.

– HO_2-constrained: A median diurnal profile of HO_2 is used to constrain the mechanism, in addition to the parameters described above. In this case, we estimate an uncertainty of ±45% for OH.

The OH- and HO_2-constrained cases are a means to explore linear and non-linear feedbacks related to RO_x radical sources, propagation, and termination, most notably by predicting the unconstrained HO_x radical.

– HO_x-constrained: We use a median diurnal profile of both OH and HO_2, from Shirley et al. (2006) to constrain the mechanism, in addition to the parameters described above. Shirley et al. (2006) report a measurement uncertainty of ±32%.

Apart from varying the constraints imposed on the model, it was also run for a) individual days, b) campaign median concentration time profiles, and c) campaign average concentration time profiles. The model was run for 18 days, 09/04–26/04/2003. Despite negligible differences in most concentration time profiles on a median and average basis, the results presented here focus exclusively on individual days and a median model, as night-time concentrations of NO – an important determinant in radical recycling rates (HO_2/RO_2+NO) – are up to 6 times higher on an average basis as compared to a median basis. As such, we consider the campaign average NO concentrations as statistical forcing rather than a realistic representation of the airmass.

Note that all concentrations, unless otherwise mentioned, are reported in parts per billion by volume (ppb_v), and all times are reported as Central Standard Time (CST i.e., Coordinated Universal Time (UTC) minus 6 (UTC-6)).

2.1 Alkanes

Alkanes were scaled using a combination of data collected via whole air canister sampling (Velasco et al., 2007) and continuous FTIR measurements (Table 1). For the days that both measurements from canister sampling and FTIR sampling are available, the data show good agreement. The concentration of each individual alkane species, relative to the sum of the alkane species (in ppbC), is effectively constant throughout the day. Diurnal profiles for each alkane species were subsequently determined by scaling continuous FTIR measurements (of effective C-H stretches) by the ratios determined from canister speciation. Based on measurement uncertainty from the GC-FID and FTIR, and the scaling methodology, we estimate uncertainty for the alkanes input as ±25%.

2.2 Alkenes

The concentrations of alkene species (Table 1) were determined using the canister data and measurements from a Fast Isoprene Sensor (FIS). A generic FIS signal was plotted against the alkene data from the canister samples accounting for the response of the FIS towards different olefin species (Velasco et al., 2007); for species in which the response factor was not available, the response factor is assumed to be unity. The scaling factors derived from the canister data are used with the continuous FIS data to generate time-resolved input parameters for the alkenes. The scaling factors for alkenes included in the box model that were not directly measured are determined using speciation profiles, as found in the literature (Harley et al., 1992). We estimate uncertainty for the alkenes input as ±25%.

2.3 Aromatics

The concentrations of aromatic species in the model are determined by direct DOAS measurements (Volkamer et al., 2004, 2005) following evaluation protocols developed

by Volkamer et al. (1998), a scaling methodology using canister data, and emissions factors (Harley et al., 1992). The compounds measured directly by DOAS and scaled using other measurements are listed in Table 1. The direct measurement of benzene is used in conjunction with canister data to scale aromatic compounds not measured by DOAS. The DOAS instruments also measured a general mono-substituted benzene signal, which is assumed to be a weighted response from ethyl benzene, n-propyl benzene, and i-propyl benzene (Axelsson et al., 1995). The compounds directly measured by DOAS, with measurement uncertainties include: toluene (±15%), benzene (±15%), o-xylene (±15%), m-xylene (±15%), p-xylene (±15%), styrene (±15%), benzaldehyde (±15%). The compounds scaled via canister speciation have estimated uncertainties of ±25%.

2.4 Oxygenated VOC

In addition to the alkanes, alkenes, and aromatic species, a number of alcohols, aldehydes, ketones, esters, ethers, and organic acids were constrained in the model, see Table 1 for the list of species and scaling methodology. Most notably, formaldehyde (HCHO) and glyoxal were measured by DOAS, both with an uncertainty of ±25%. Based on the scaling methodology employed here, we estimate that the uncertainty for the oxygenated compounds not directly measured is ±50%.

Note that for the oxygenated compounds not directly measured, aerosol related loss processes – as discussed for glyoxal in Volkamer et al. (2006), for example – are not included.

2.5 Dilution

For a more detailed discussion of the methodology employed to constrain the model for dilution, refer to Volkamer et al. (2007). A summary is provided here. The dilution parameter was estimated using a combination of two approaches: Using traffic counts and measured concentrations of CO (traffic-CO) to generate a proxy for the ris-

ing planetary boundary layer (PBL), and by matching predicted photochemical HCHO with observations. If only the traffic-CO approach is used, then uncharacteristic chemical accumulation in the code is observed. The increased dilution as a result of the HCHO modeling eliminates this unrepresentative accumulation of secondary products (i.e., oxidized volatile organic compounds, OVOC).

2.6 Photolysis rates of reactions

The photolysis frequencies for O_3 (J_{O_3}, ±25%), NO_2 (J_{NO_2}, ±15%), HCHO (J_{HCHO}, ±15%), CH_3CHO (J_{CH_3CHO},±15%), and HONO (J_{HONO},±15%) are constrained by measurements (Volkamer et al., 2005). The values for J_{HONO} have been multiplied by 1.43 to match recent absolute measurements made by Wall et al. (2006) consistent with results presented in Volkamer et al. (2007). All of the measured J-values were multiplied by 1.08 to account for surface albedo corrections. The code calculates photolysis rates solely as a function of solar zenith angle, which does not account for cloud coverage, scattering in the atmosphere, and the albedo of the earth's surface. As such, the photolysis rates are corrected using a factor that is based on the average difference between the calculated and measured values for J_{NO_2}. Calculations were initially performed using clear sky conditions at a latitude of 19°21′32″ N and a longitude of 99°4′25″ W.

3 Results and discussion

3.1 Individual day modeling

The modeling results are quantified in terms of radical initiation, propagation, and termination routes for individual days for the i) HO_x-unconstrained (left) and ii) HO_x-constrained cases (right) in Table 2 – other parameters are also included, and are discussed in greater detail below. Note that the meteorology classification listed in the

last row of each of the tables is taken from de Foy et al. (2005). In the event that the continuous collection of data was interrupted, the data gaps were filled by either a) extrapolating based on the median concentration profiles, or b) linearly correlated based on the final measurement before and the first measurement following the gap. Note the variability in radical initiation and cycling on different days. For instance, we report total RO_x radical initiation as low as 219×10^5 molec. cm^{-3} s^{-1} on 18/03 and as high as 808×10^5 molec. cm^{-3} s^{-1} on 15/03. Similarly, we observe the lowest rates of recycling on 18/03; however, we observe the highest rates of recycling on 23/03 because of comparable initiation coupled with higher NO concentrations as compared to 15/03.

3.2 OH reactivity

For each of the cases described above, with the exception of the HO_x-constrained case, OH loss is equal to OH production within τ_{OH}<0.1 s i.e., OH is in steady state. The modeled and median measured OH reactivity are shown in the bottom panel of Fig. 2; the total OH reactivity predicted by the model is about 110 s^{-1} during morning rush hour and a value of roughly 20–25 s^{-1} during the day and between 45–50 s^{-1} at night. These values are consistent with those measured by Shirley et al. (2006); however, there is a significant difference between measured and modeled values from 05:00–07:00, when NO_x values are highest. The uncertainty in the total OH loss measurement is highest under high NO_x conditions (Shirley et al., 2006). The degree of constraint imposed on the mechanism by inputs in terms of OH reactivity is shown in the upper panel of Fig. 2. Most notably, the fraction of OH reactivity due to reaction with unconstrained parameters linearly increases in the morning around 08:00 until 12:00. This increase is roughly 1 h after the onset of photochemical processing and due to the oxidation of primary VOC, resulting in the formation of secondary products. The formation of secondary products and their subsequent oxidation results in an increase of unconstrained OH loss of roughly 5% per h, reaching a maximum of 25%. The decrease in the fraction of OH loss from unconstrained parameters around 12:00 reflects the venting of the MCMA, is consistent with an observed decrease in new OH radical

production (Volkamer et al., 2007), and reflects the dilution implemented in the code (see Volkamer et al., 2007 for details).

3.3 HO_x: measured vs. modeled[2]

The HO_x-unconstrained model accurately predicts the diurnal profile of both OH and HO_2, as shown in Fig. 3A,C. When compared to a lower limit of measured OH values (based on a 0.01 ppt_v statistical offset, see Volkamer et al., 2007), the model predicts OH within measured and modeled uncertainties for the entire day (Fig. 3A). In the early morning, between 06:00–07:00 (i.e., rush hour), the model under-predicts OH radicals by roughly a factor of 2; however, because the concentrations are so low at this time, the model is still within measured uncertainties. Similarly, a slight and consistent under-prediction is observed in the evening after 18:00. The model over-predicts OH concentrations in the afternoon by a maximum of 20%.

The model under-predicts the concentration of HO_2 for the entire day, and most notably between midnight and 10:00. The measured-to-modeled ratios are consistently above 10 before 07:00. The predicted concentrations do not fall within the measurement and modeled uncertainty until around 10:00. The model predicts HO_2 within modeled and measured uncertainties between 10:00 and 18:30. Thereafter, the ratio of measured-to-modeled concentrations starts increasing and varies between 5–10 for the remainder of the day.

The median concentrations of predicted OH and HO_2 from individual day modeling show good agreement with the predicted OH and HO_2 from the HO_x-unconstrained

[2]The measured OH and HO_2 concentrations used for comparison are reported in Shirley et al. (2006); however, it is possible that there will be an adjustment to the HO_x measurements that would increase the reported concentrations by a factor of up to 1.6 (W. H. Brune, personal communication). To account for this, we have included, where appropriate, both the reported measured HO_x concentrations and these values multiplied by 1.6. It is also worth noting that the potential increase in HO_x concentrations will generally have a minor effect, if any, on the conclusions drawn here.

model of campaign median concentration inputs of HO_x sources and sinks, as shown in Fig. 3A and C, respectively. A linear regression of individual day OH and HO_2 modeled predictions versus measured values yields the following relationships:
$[OH]_{model}$ = 0.73*$[OH]_{meas}$ + 0.02 ppt, R^2=0.98, and
$[HO_2]_{model}$ = 0.74*$[HO_2]_{meas}$ − 2.79 ppt, R^2=0.96.

Despite what appears to be a good correlation between measured and modeled values, a more thorough analysis shows these results belie the lack of radicals at high concentrations of NO_x: For both OH and HO_2, the measured-to-modeled relationship is predominantly determined by higher concentrations in the afternoon. As such, the linear regression is skewed in favor of times when the model more accurately predicts HO_x concentrations (which, is also at low NO_x conditions).

When the model is constrained for HO_2 (Fig. 3B), it is unable to predict the diurnal profile of OH. As a result of the HO_2 forcing, the model over-predicts the concentration of OH for the majority of the day, most notably in the morning 04:00–10:00, and at night, 19:00–24:00. However, we do observe overlap in the observed and predicted concentrations during much of the day, 10:00–18:00. The uncharacteristic diurnal profile of OH and the high concentrations reflect the coupling between HO_2 and OH via NO.

In the case of the OH forcing (Fig. 3D), the effect on modeled HO_2 concentrations is less direct, particularly because it involves the entire RO_x cycle; however, the effects of the OH forcing are significant. Most notably, from midnight to 06:00 and again from 18:00–24:00, the measured and modeled HO_2 are in much better agreement. Conversely, the model still drastically under-predicts the concentrations of HO_2 shortly after sunrise until 09:30. This suggests that the gas-phase mechanism is lacking a HO_2 (or RO_2) production term.

The exercise of forcing OH and HO_2 concentrations in the mechanism is valuable, as it can help elucidate shortcomings in the mechanism. The HO_2-forcing suggests that the gas-phase mechanism – particularly under high NO_x conditions – lacks either a significant HO_2 source that does not form OH or an HO_2 source and OH sink. It is also

possible that the mechanism lacks a large sink for OH; however, this is inconsistent with the relatively small differences between measured and modeled OH loss (Fig. 2). Similarly, high uncertainty in the OH loss measurements at high NO_x conditions complicates drawing conclusions from this time period. Because the modeled predictions of OH show good agreement with measurements in the HO_x-unconstrained case, and because of high uncertainty in the OH loss measurements, a large missing gas-phase OH sink seems unlikely. Similarly, the modeled OH in the HO_x-unconstrained case is generally under-predicted, which does not lend support to the argument that the mechanism has a missing sink for OH.

3.4 HO_2/OH vs. NO

Apart from absolute HO_x concentrations, the ratio of HO_2 to OH as a function of NO is a useful relationship to test our understanding of HO_x cycling (Fig. 4). We compare measured and modeled HO_x ratio vs. NO on both a campaign median basis and an individual day basis. For the sake of comparison, we binned OH, HO_2, and NO values based on 10 different ranges of NO concentrations. Also note that the error bars shown for the modeled scenarios capture the variability of individual days as shown in Table 2.

We observe a similar relationship between the HO_2/OH ratio and NO for both the measured and modeled values; however, there are significant differences at high NO. The modeled HO_2/OH ratio is lower than the measured ratio by roughly a factor of 4 at NO concentrations of 100 ppb. The difference narrows to a factor of 2–3 between NO concentrations of 10–100 ppb, and is ≤2 for NO concentrations between 1–10 ppb. The larger differences between modeled and measured HO_2/OH ratio at high NO occurs in the morning and at night, when the model most drastically underestimates the concentrations of HO_2.

The "missing reactivty" noted above in Sect. 3.3 is also evident in the HO_x ratio as a function of NO. The measured HO_x ratio has a shallower slope with respect to NO than the modeled ratio does. The slope of the graphs in Fig. 4 yield the NO power dependence. We expect a dependence of between 1 to 2 (Shirley et al., 2006);

however, the measured values of the HO_2-to-OH vary as NO to the power of 0.36, and the modeled values vary as NO to the power of 0.64, nearly a factor of 2 increase. The lower-than-expected NO power dependence is tentatively attributed to more efficient HO_x cycling in VOC chemistry ad is consistent with laboratory observations (Bloss et al., 2005a,b).

The HO_2/OH ratio vs NO relationship is also useful in determining the effects of using median diurnal profiles from campaign data for modeling. Legitimate concerns exist regarding conclusions drawn from the use of average or median diurnal profiles of radical sources and sinks, particularly because the characteristics of fast HO_x–NO_x chemistry may not be captured. To test our use of campaign median data and day-to-day variability thereof, we also used the model to predict HO_x concentrations on a "high NO_x" day (NO_{max}=220 ppb) and a "low NO_x" day (NO_{max}=24 ppb). The modeled HO_2/OH results are also shown in Fig. 4; the individual day results – for both the measurements and the modeling – show good agreement with the campaign median results, confirming the utility of modeling on a campaign median basis.

3.5 Predicting RO_2

Organic peroxyl radicals play a major role in atmospheric processes, most notably in its reaction with NO yielding NO_2, adding to O_3 production. Unfortunately, ambient measurements of RO_2 are difficult, and unavailable from MCMA-2003. As such, we use MCMv3.1 and the different constrained cases to understand the model's prediction of RO_2 in relation to HO_x.

The predicted concentrations for RO_2 in the different modeling scenarios are shown in Fig. 5. The HO_x-constrained (not shown) and OH-constrained cases predict the same concentration of RO_2 because the effects of the OH constraint supersede any effects of the HO_2 constraint. The more direct coupling between OH and RO_2 radicals is also evident when comparing the HO_x-unconstrained and constrained cases: the higher concentrations of RO_2 from 10:00–16:00. in the unconstrained case are coincident with the model's over-prediction of OH, noted previously and shown in Fig. 3.

The RO_2/HO_2 ratios (shown in Fig. 5b vs NO) are another metric used to understand the prediction of RO_2 as it relates to HO_x. In each of the modeled scenarios in steady state, the RO_2/HO_2 ratio is between 0.7–1, whereas in the fully constrained case, the ratios are significantly lower and drop below 0.2 when NO>7 ppb. As mentioned previously, the coupling between OH and RO_2 is more important than that between HO_2 and RO_2; as such, the lower-than-expected ratios are a function of the fixed OH counter-balancing any effects that a fixed HO_2 concentration may have. We consider the predicted RO_2 concentration in the HO_x-constrained case as a lower limit.

3.6 Chain length

Chain length is broadly defined as the number of times that a hydroxyl radical will be regenerated via the RO_x cycle (Fig. 1); it is a quantitative measure for the number of VOC oxidized per OH radical produced from initiation routes. As such, the radical chain length is a parameter that captures the characteristics of the fuel (i.e., VOC) in its oxidative environment. The chain length is also an effective means to assess the relative importance of new radical production relative to radical turnover in the MCMA. We define a parameter for chain length, n(OH), as:

$$\mathrm{n(OH)} = \gamma_{\mathrm{OH}} \left[\frac{\Sigma \mathrm{OH_{new}} + \text{propagated OH}}{\Sigma \mathrm{OH_{new}}} \right], \quad (1)$$

where γ_{OH} is the fraction of OH entering the radical cycle:

$$\gamma_{\mathrm{OH}} = \frac{(\mathrm{OH} \rightarrow \mathrm{RO_2}) + (\mathrm{OH} \rightarrow \mathrm{HO_2})}{\text{total OH loss}}. \quad (2)$$

There are numerous parameters used to calculate chain length found in the literature (e.g., Wagner et al., 2003; Seinfeld and Pandis, 1998; Emmerson et al., 2007; Stroud et al., 2004; Martinez et al., 2003). Most parameters for chain length assume that a single OH radical will cycle through at least once (i.e., n(OH)=1). If OH sinks are strong

enough or if VOC concentrations are sufficiently low, we conclude that a single radical may not complete the cycle before being removed from the system, and have therefore added the γ_{OH} term. While this scenario (i.e., n(OH)<1) is unlikely in a polluted environment such as Mexico City, it is nonetheless an important adjustment to remain consistent in our calculation of n(OH) as a quantitative measure of chain length.

The calculation of the chain length parameter is sensitive to the definition of cycling terms, including initiation, propagation, and termination. This requires careful accounting of the reactive pathways; essentially, we assign a value (in terms of radical flux) to every arrow in Fig. 1, and each arrow is a summation of many reactions. The definitions employed here are similar to those used by Wagner et al. (2003):

- New radical production (i.e., initiation) is the breakdown of a closed shell molecule into two radicals or as the conversion of O_3 or NO_3 into a RO_x species;
- Propagation is the transformation of one RO_x species into another;
- Termination (i.e., radical sinks) is the formation of a closed shell molecule from the reaction of two radicals; and,
- The mechanism contains certain species that are in fast equilibrium with radicals, such as PAN. For these compounds, a net term is calculated: the net parameter is then appropriately classified as either production or termination.

In contrast to Wagner et al. (2003), we do not include:

- "delayed propagation": fast radical-radical reactions form a radical reservoir that subsequently photolyzes to yield two radicals; and,
- HONO net flux: The production of HONO from the reaction between OH and NO is subtracted from the production of OH from HONO photolysis. This term is then lumped into ΣOH_{new}.

We have assessed the effect of including a "delayed propagation" term in the calculation of n(OH). When including the net flux from radical-radical recombination reactions and the subsequent photolytic decomposition reactions for all the appropriate species (i.e., hydroperoxide, organic peroxides, and oxygenated compounds e.g., aldehydes), we observe a modest increase in n(OH) (not shown); however, this a function of accounting, and not a chemical manifestation of radical cycling. The differences are only observed during the day-time, as it is OVOC formed from the processing of primary emissions at sunrise that make the greatest impact on the delayed propagation accounting. Wagner et al. (2003) uses a similar net flux approach in the treatment of HONO. A potential problem associated with using the net flux approach for HONO is a negative term in the summation of ΣOH_{new}; that is, whenever HONO formation is larger than HONO photolysis, the contribution of new OH to ΣOH_{new} may be a negative number, which does not make physical sense. Ultimately, our definition of n(OH) as a parameter for chain length does not include "delayed propagation;" or a net flux approach for HONO accounting; in our case, the processes are treated discretely as either termination or new radical production.

Having defined the various radical reaction pathways, we use the grouped terms to calculate chain length. Rather than calculate a single OH chain length based solely on the "long" chain [L: $OH \rightarrow RO_2 \rightarrow RO \rightarrow HO_2$], we also consider the direct cycle between between OH and HO_2 i.e., the "short" chain (S). That is:

$$n(OH)_{total} = \alpha_{OH \rightarrow HO_2} n(OH)_S + \beta_{OH \rightarrow RO_2} n(OH)_L, \quad (3)$$

where

$$\alpha_{OH \rightarrow HO_2} = \frac{OH \rightarrow HO_2}{OH \rightarrow HO_2 + OH \rightarrow RO_2}, \text{ and} \quad (4)$$

$$\beta_{OH \rightarrow RO_2} = 1 - \alpha_{OH \rightarrow HO_2}. \quad (5)$$

The first term in the chain length calculation, ΣOH_{new}, is the sum of all new RO_x radical production, weighted as OH equivalents i.e., accounting for conversion efficiencies

between $RO_2 \rightarrow OH$ and $HO_2 \rightarrow OH$. New HO_2 and RO_2 radicals are major contributors to the balance of new radicals, but only the percentage of new radicals that are converted into OH via cycling are included in the summation; new RO radicals contribute less than 1% to new radical production (Volkamer et al., 2007). To account for the percentage of new HO_2 and new RO_2 radicals that contribute, we define them as OH equivalents:

$$[OH_{eq}]_{HO_2} = \gamma_{HO_2} * [HO_2]_{new}, \quad (6)$$

$$[OH_{eq}]_{RO_2} = \gamma_{RO_2} * [RO_2]_{new}, \quad (7)$$

where γ_{HO_2} and γ_{RO_2} are the conversion factors of the respective species into OH:

$$\gamma_{HO_2} = \frac{HO_2 \rightarrow OH}{\text{total } HO_2 \text{ loss}}, \quad (8)$$

$$\gamma_{RO_2} = \gamma_{HO_2} * \gamma_{RO} * \frac{RO_2 \rightarrow RO}{\text{total } RO_2 \text{ loss}}, \text{ and} \quad (9)$$

$$\gamma_{RO} = \frac{RO \rightarrow HO_2}{\text{total RO loss}}. \quad (10)$$

We calculated n(OH) and γ for individual days in both the HO_x-constrained and HO_x-unconstrained cases; the median values are shown in Fig. 6. In the HO_x-constrained case, cycling is high in the morning, with a peak of 20 around 06:45 and decreasing to 7 over the next hour. From 10:30 to 14:30, the n(OH) is between 4 and 6. Conversely, there is no morning peak evident in the HO_x-unconstrained case. This difference in n(OH) is coincident with previously noted missing reactivity shortly after sunrise and during rush-hour. The n(OH) for the HO_x-unconstrained individual day modeling reaches a high value of about 4 around 05:00 and is in the range of 2.5–4 throughout the day. The peak difference in chain length values occurs at 06:40, at which time the

median value for the constrained case is a factor of 6 higher than the unconstrained modeling.

The conversion factors, γ_{RO_x} shown in the upper panel of Fig. 6, provide a means to understand cycling via an alternative approach. The conversion factors are a measure of radical propagation efficiency relative to termination. We treat radical cycling as an exponential decay process and define a separate parameter to determine chain length, (ω), so that:

$$-\prod \gamma_{RO_x}{}^{\omega} \doteq \frac{1}{e}, \text{ and} \quad (11)$$

$$\omega = -[\ln \prod \gamma_{RO_x}]^{-1}, \text{ where} \quad (12)$$

$$\gamma_{RO_x} = \gamma_{OH} \times \gamma_{RO_2} \times \gamma_{RO} \times \gamma_{HO_2} \quad (13)$$

The median wheel value for the HO_x-constrained cases is shown in Fig. 6. The agreement between n(OH) and ω is a measure of our understanding of radical cycling. In principle, the parameters should be the same; however, they show significant differences between 04:00–10:00, and again after 14:00. The parameters have different perspectives with regard to radical cycling: the n(OH) focuses on propagation and initiation, while ω focuses on propagation and termination. To bring the parameters into agreement, the mechanism requires: 1) additional radical sources to lower the chain length; 2) an increase in the radical conversion efficiencies and hence the wheel, which can be achieved by fewer radical sinks (i.e., more efficient propagation) or, 3) a combination of 1 and 2. During the period of most significant disagreement between *n(OH) and ω^{*}, the product of the γ-values varies between 0.6–0.7 (see upper panel of Fig. 6); in order for ω to reach cycling values of 20, the product of the γ-values must approach 0.95, which is inconsistent with our current understanding of organic peroxyl and hydroperoxyl radical kinetics. It should be noted that any change in the radical conversion efficiencies of $RO_2 \rightarrow RO$, $RO \rightarrow HO_2$, and $HO_2 \rightarrow OH$ will have a non-linear effect on the calculation of n(OH), as it will increase the contribution of new HO_2 and/or new RO_2 to the ΣOH_{new} term.

3.7 OH production and loss: Measurement imbalance

The hydroxyl radical is a short-lived species in the atmosphere, and is in steady-state on a time scale of 0.1 s. Shirley et al. (2006) note the balance observed in median OH production, P(OH), and OH loss, L(OH). The only notable exception is between 07:00–08:00 when OH production is twice OH loss. P(OH) and L(OH) are defined here as:

$$P(OH) = k_{HO_2+NO}[HO_2][NO] + OH_{new}, \text{ and} \quad (14)$$

$$L(OH) = k_{OH+NO_x}[OH][NO_x] + k_{OH+VOC}[OH][VOC]. \quad (15)$$

The production of OH via reaction between HO_2 and NO accounts on average for more than 80% of P(OH). OH_{new} is equivalent to initiation i.e., the generation of a OH radical from the breakdown of a closed shell species e.g., O_3, and is discussed in more detail elsewhere (Volkamer et al., 2007). The extensive suite of data, including HO_x and OH loss measurements, provides the means to calculate both OH production and loss throughout the campaign, as shown in Fig. 7-A. The difference between median P(OH) and L(OH), $L(OH)_{med} - P(OH)_{med}$, is shown with a 2σ experimental uncertainty, which is duplicated from the work by Shirley et al. (2006). We have also included the median difference between individual measurements, $(L(OH)_{ind} - P(OH)_{ind})_{med}$, and plotted it with 1σ standard deviation i.e., the statistical scatter of the difference between production and loss on an individual basis. Even though the L–P difference plots are similar, the blue error bars emphasize the considerable scatter of individual measurements, and reflect what we consider an imbalance in the measurements. In other words, the "balance" between median production and median loss observed by Shirley et al. (2006) is a function of averaging large statistical scatter, rather than a balanced set of measurements bound by experimental certainty.

To illustrate this more clearly, the difference between OH production and loss from individual measurements as a function of NO is shown in Fig. 7-B. The difference is

shown as the absolute value of [P(OH)−L(OH)]/P(OH), and values are further separated by 1) P(OH)>L(OH), and 2) P(OH)<L(OH). The 2σ experimental uncertainty is taken as 55% (Shirley et al., 2006), and represented as a dotted line in the figure. Any point below this line represents a balance between production and loss within experimental uncertainty, whereas any point above the line represents an imbalance in the measurements. By this estimate, 55% of the individual measurements fall outside of the experimental uncertainty – rather than the expected 33% based on a 2σ confidence level – 75% of which are at values of NO lower than 10 ppb (i.e., when confidence in the measurements is highest).

We are not challenging the accuracy of the HO_x concentration or OH loss measurements, which are of the highest quality attainable to date. The noted imbalance is also independent of the HO_x calibration. The lack of agreement between OH production and OH loss has drastic implications for any box model. Our MCM box model is simply unable to predict the observed HO_2 concentrations because of high concentrations of NO_x in the same air mass. Notably, we use measurements taken at similar heights. Although unlikely, the imbalance in the measurements may be the result of micrometerological phenomena, with particular emphasis on NO_x, which directly challenges the assumption that the air mass is homogeneously mixed.

3.8 Ozone production

Ozone formation is essentially a competition process between VOC and NO_x for OH (Seinfeld and Pandis, 1998). Net instantaneous ozone production, $P(O_3)$, is a measure of ozone formation as a result of NO oxidation via reaction with HO_2 or RO_2, yielding NO_2 and OH or RO, respectively. The production rate also accounts for radical loss channels forming HNO_3 and RNO_3. The net instantaneous O_3 production is calculated as:

$$P(O_3) = k_{HO_2+NO}[HO_2][NO] + \Sigma k_{RO_2+NO}[RO_2][NO] - k_{OH+NO_2+M}[OH][NO_2][M] - P(RNO_3)$$

The median $P(O_3)$ diurnal profiles for the individual days and the median model in the HO_x-constrained and HO_x-unconstrained scenarios are shown in Fig. 8. The median profile of $P(O_3)$ as calculated using solely measured HO_2 is also shown.

The median-model HO_x-constrained, median of individual day HO_x-constrained modeling, and HO_2-measured cases exhibit similar profiles for $P(O_3)$, with a peak at 08:00 of 89, 88, and 50 ppb h^{-1}, respectively. The median-model HO_x-unconstrained and individual day HO_x-unconstrained modeling show similar profiles, but are very different from the other 3 cases shown. The timing of the peak ozone production is shifted by about 2 h, and shows a much less pronounced peak of roughly 45 ppb h^{-1}. We consider the profiles for both the HO_x-constrained cases as lower limits because of a lower-than-expected RO_2/HO_2 ratio, as shown in Fig. 5-B. If a RO_2/HO_2 ratio of unity is assumed, the magnitude of $P(O_3)$ increases to well above 100 ppb h^{-1}.

The differences observed in the $P(O_3)$ profiles, most notably between 06:00 and 10:00, are coincident with the aforementioned missing reactivity. The under-estimation of HO_x radicals in the unconstrained code manifests itself in both the magnitude and timing of peak ozone production. Despite the fact that the various profiles come into good agreement by 10:00, the measurements indicated that the bulk of NO→NO_2 conversions take place before that time. The upper panel of Fig. 8 quantifies the effects of the missing reactivity on the oxidative capacity of the Mexico City atmosphere: The HO_x-constrained case predicts a minimum of 75% greater cumulative ozone production than the unconstrained case throughout the day, with a factor of 5 difference in the early morning at the onset of photochemical processing.

3.8.1 VOC_R and NO_x

We use an ozone isopleth-type graph in Fig. 9 to illustrate the relationship between $P(O_3)$ and VOC_R and NO_x-these plots are similar to those shown in Kleinman et al. (2005). We observe very high values for both VOC_R and NO_x in Mexico City; much

ACPD
8, 5359–5412, 2008

higher than in all US urban airmasses e.g., Houston, Nashville, New York, and Phoenix Kleinman et al. (2005). We observe a near-constant upward sloping relationship between VOC_R and NO_x, indicating the colocation of VOC and NO_x sources.

The differences in measured and predicted HO_x radical concentrations yield different $P(O_3)$ values, as shown in Fig. 9-A and B. In panel B, there is a two-fold increase in the number of points with a predicted $P(O_3)$>40 ppb h^{-1} as compared to the HO_x-unconstrained case.

Theory predicts that $P(O_3)$ will reach a maximum at low NO_x concentrations and decreases at higher NO_x concentrations: We observe this in the HO_x-unconstrained case, however, we do not observe this to be true in the HO_x-constrained case. The VOC loadings in Mexico City are sufficiently high at high NO_x concentrations to perpetuate radical cycling, rather than allowing the termination pathways via NO_x reactions to dominate. The measured HO_x concentrations at concurrently high VOC and NO_x loadings characterize a previously unidentified scenario for ozone production rates.

Kleinman et al. (2005) also employ a novel parameter L_N/Q to understand the VOC and NO_x limitations of ozone production, where L_N is the sum of RO_x radical loss rates due to reaction with NO_x and Q is the summation of new radical production. While our explicit model is ideally suited to predict this parameter, and compare to values presented by Kleinman et al. (2005), the HO_x-constrained code presents a problem because it is unbalanced with regard to radical production and destruction. This imbalance results in higher than expected values for L_N, resulting in values for the L_N/Q parameter well above 1. These values do not make physical sense, and as such, we are unable to use the L_N/Q parameter in the same manner as Kleinman et al. (2005) to draw conclusions about the VOC and/or NO_x sensitivity of the MCMA.

Our near-explicit code does, however, provide the means to test some of the basic assumptions employed to derive the L_N/Q parameter to the MCMA. The approximation of L_N being equivalent to the flux from the reaction of OH with NO_2 i.e., that the formation of organic nitrates via reaction of RO_2 with NO is negligible, under-estimates L_N by some 15–30% throughout the day. In determining the relationship between L_N/Q

relative to VOC reactivity and NO_x reactivity, Kleinman et al. (2001) also make the following assumption. In the limit that chain propagation is much more important than chain initiation and termination:

$$k_{OH+VOC}[OH][[VOC]=k_{HO_2+NO}[HO_2][[NO] \quad (17)$$

Even though the VOC loadings are high and radical cycling is fast in the MCMA, this assumption breaks down in the high NO_x environment in the MCMA. Based on our model, by not accounting for other radical pathways i.e., OH→HO_2 (P5 in Fig. 1) or OH termination (T1 in Fig. 1) in their approximation, Kleinman et al. (2001) introduce an uncertainty of about 20%. In the HO_x-constrained model, the measured concentrations of HO_2 are higher than in the unconstrained case, and the radical flux of HO_2→OH is subsequently much higher than OH loss via reaction with VOC. As such, the assumption by Kleinman et al. (2001) introduces a minimum uncertainty of 20%, and a maximum of a factor of 5 (i.e., 500%) in the HO_x-constrained case. Combining the uncertainty in the determination of L_N and the imbalance in the assumption relative to OH production and loss, we estimate a lower-limit of uncertainty in the L_N/Q parameter of some 30%. Furthermore, this does not account for any uncertainty in the Q parameter; depending on the time of day, O_3 and HCHO photolysis and O_3/alkene reactions account for 29–65% of the value of Q (Volkamer et al., 2007). Despite these limitations, an expanded L_N/Q concept can conceivably be applied to the MCMA.

3.8.2 Missing OH reactivity

Recent findings indicate that POA upon dilution from the tailpipe of a car to atmospheric conditions may act as a source of semivolatile hydrocarbons in urban air, so-called semi-volatile organic compounds (SVOC) and intermediate volatility organic compounds (IVOC) (Donahue et al., 2006; Robinson et al., 2007). The chemical identity of these hydrocarbons is unclear, and, as such, SVOC and IVOC are not represented in MCM. These species could be relevant to SOA formation (Robinson et al., 2007) and possibly ozone production. We estimate here for the first time the possible

contribution of SVOC and IVOC to OH reactivity to assess whether the gap between modeled and measured reactivity can be attributed to these species. We calculated the OH reactivity of SVOC and IVOC by estimating the amount of each in the gas phase using POA measurements (Salcedo et al., 2006): SVOC + IVOC = 4*POA + 7.5*POA. Here, we parameterized the data from Fig. 1A in Robinson et al. (2007) to account for the effects of variable partitioning depending on POA partitioning mass. We used a molecular weight of 250 g mol^{-1}, consistent with Robinson et al. (2007), to convert μg m^{-3} to units of molec cm^{-3}. Using this concentration, and a generic rate constant for reaction with OH radicals of 4×10^{-11} cm^3 molec^{-1} s^{-1} reported by Robinson et al. (2007), we calculate the corresponding OH loss rate. The results are plotted as an overlay in Fig. 2. Using this methodology, we observe a modest increase of 4–14 s^{-1} of OH reactivity (about 10% of the measured value). The existence of SVOC and IVOC is consistent with the observation of a gap in OH reactivity, though insufficient to obtain closure. Future studies will need to demonstrate whether the parameterization of SVOC and IVOC from diesel fuel provides for a meaningful extrapolation to ambient POA. It appears, however, from this analysis that SVOC and IVOC make a sufficiently large contribution to OH reactivity to be potentially relevant to O_3 formation.

Of particular note, we observe a correlation of missing OH reactivity and the difference in the chain length parameters, n(OH) and ω, as shown in Fig. 10. The links between radical (re)cycling and missing reactivity are an important area for consideration in future work, particularly related to the ongoing analysis of the Mexico City airmass using data collected in 2003 and in the 2006 MILAGRO campaign. It is clear from Fig. 10 that shortcomings remain in our understanding of HO_x radical cycling.

4 Comparison to other studies

4.1 Radical budgets

The MCMv3.1 has only recently been used in similar detail to quantify radical fluxes for initiation, propagation, and termination. In Part 1, Volkamer et al. (2007) discuss new radical production rates to other airmasses, noting both the homogeneity of radical sources in the MCMA and the higher production rates. The radical fluxes for cycling routes that we report for both the HO_x-unconstrained and HO_x-constrained cases are considerably higher than those reported elsewhere (Emmerson et al., 2007, 2005; Platt et al., 2002). Apart from the RO→HO_2 route, the radical flux from one RO_x radical to another is roughly 1.5–3 times larger in the MCMA compared to the cleaner sub-urban airmass observed during the TORCH campaign, and the semi-polluted atmosphere in Birmingham during the PUMA campaign. The radical flux of propagation pathways is higher for the MCMA due to higher NO_x concentrations and higher VOC concentrations. The RO→HO_2 flux in the MCMA is comparable to the value reported for Birmingham for 2 reasons: 1) at the high concentrations of NO observed during MCMA-2003, the conversion efficiency for the RO_2→RO route is lower due to the formation of organic nitrates (RNO_3). This yields fewer RO radicals, meaning a lower flux into HO_2. 2) We observe a much higher rate of thermal decomposition of RO radicals back into RO_2 radicals. A direct comparison with the BERLIOZ campaign is difficult because the radical production rates are distinguished only by production and destruction.

4.2 Missing HO_x reactivity

The under-prediction of OH and HO_2 in our HO_x-unconstrained mechanism is an indication of missing reactivity. This missing reactivity has also been observed in a variety of environments, including atmospheric chamber studies (Bloss et al., 2005a,b), the upper troposphere (Folkins et al., 1997; Tan et al., 2001; Faloona et al., 2000), and other urban areas (Martinez et al., 2003; Ren et al., 2003). Shirley et al. (2006) em-

ploy the RACM mechanism to study the MCMA and do not observe the same missing reactivity at high NO_x concentrations, and report that the measured-to-modeled ratios during rush hour for OH and HO_2 are 1.07 and 1.17, respectively. Conversely, Ren et al. (2003) note an increasing measured-to-modeled ratio with increasing NO. At NO concentrations greater than 10 ppb, their model under-predicts HO_2 by a factor of 2–20, similar to what we observe in the MCMA. To explain the difference, they suggest unknown HO_x sources that increase with NO, or a shortcoming in HO_x-NO_x chemistry. Based on our analysis using the detailed MCMv3.1 and the chain length cycling parameters, n(OH) and ω, we conclude that there is a significant missing source for HO_2 and smaller one for OH. On the other hand, it is also clear that the introduction of a missing source for HO_2 must be accompanied by a pathway that does not form OH via reaction with NO (i.e., a sink for HO_2 radicals) or be accompanied by an efficient OH loss mechanism consistent with results in Sect. 3.8.2 because the predicted OH concentrations are generally very good.

The very high NO_x concentrations observed during MCMA-2003 makes our study unique amongst those employing the Master Chemical Mechanism. We have extended the NO_x range over which MCM has been tested and this extension demonstrates the incomplete understanding of HO_x chemical cycling at high NO_x beyond experimental doubt. In other studies employing the MCM, the peak NO_x concentrations are roughly 30 ppb for PUMA-summer, 30 ppb for BERLIOZ and 25 ppb for the TORCH campaign. High concentrations of NO_x were observed during the winter months of the PUMA campaign (140 ppb), however, HO_2 measurements were largely unavailable to compare with predicted values. The median peak NO_x concentration employed here is about 130 ppb, with some days as high as 250 ppb. As such, the noted missing reactivity, while difficult to compare directly with other field campaign analyses employing the MCM, presents confirmation at previously unstudied high NO_x conditions.

4.3 Defining chain length

The chain length parameter n(OH) is widely used as a quantitative measure of radical cycling. Even though the broad definition of chain length as the number of VOC that one OH radical oxidizes is consistent, the equations used to calculate it varies significantly. We evaluate several of these equations here. Seinfeld and Pandis (1998) define it as:

$$n(OH)_{Seinfeld/Pandis} = \frac{\text{new OH} + \text{old OH}}{\text{new OH}}, \quad (18)$$

where "old" OH is defined as recycled or propagated OH, a similar equation to the one employed here. On the other hand, in the TOPSE campaign, Stroud et al. (2004) calculate chain length as:

$$n(OH)_{TOPSE} = \frac{P(OH)_{cycling}}{L(RO_x)}, \quad (19)$$

where $P(OH)_{cycling}$ is OH radical production from propagation routes (i.e., $HO_2 \rightarrow OH$) only and $L(RO_x)$ is the sum of all radical losses. In a slightly different approach, Emmerson et al. (2007) calculate chain length as:

$$n(OH)_{TORCH} = \frac{P(OH)_{HO_2 \rightarrow OH}}{\text{new OH}}, \quad (20)$$

where the OH production term is solely defined by the HO_2 propagation route and new OH is the same as I1 in Fig. 1.

As part of the Southern Oxidants Study (SOS), Martinez et al. (2003) use the following equation:

$$n(OH)_{SOS} = \frac{[OH] * OH_{reactivity} - L(HO_x)}{L(HO_x)}, \quad (21)$$

The range of equations for OH radical chain length make comparisons between airmasses of different VOC and NO_x loadings extremely difficult. For instance, at peak NO_x concentrations around 07:00 we calculate a chain length using the equations defined above and obtain the following, with the corresponding identifier: 45-TORCH, 25-Seinfeld/Pandis, 20-this work, 19-TOPSE, and 14-SOS. By 12:00, they come into better agreement, but the range of values is still 2–6. Clearly, there is a need for a formalized equation to match the definition of chain length for sufficiently conclusive comparisons between airmasses. In the case of the equation provided by Seinfeld and Pandis (1998), they do not account for the sink of OH radicals, as defined by us as γ_{OH}. Similarly, in applying their equation, we must assume that "new OH" is equivalent to ΣOH_{new}. In the TOPSE and SOS calculation of chain length, the role of new radical formation is folded entirely into radical propagation and termination. Ultimately, both of these assumptions over-simplify the conversion efficiency between RO_2 and HO_2 to OH. The major deficiency in the calculation of chain length used in the TORCH campaign is the over-simplification of radical initiation. As mentioned previously, when accounting for "new OH", one must account for the sum of new radicals entered into the system. This is particularly important because the sum of new RO_x radical production is considerably larger than new OH radical production (see Table 2, or Volkamer et al., 2007). While each of the equations above provides a qualitative understanding of radical propagation relative to initiation and/or termination, they lack an explicit and quantitative determination of OH radical chain length. The flexibility of MCM provides us with the means to account for each of the radical initiation, propagation, and termination pathways (Fig. 1). Similarly, it makes no assumptions about the VOC or NO_x environment. As such, we are confident that our explicit calculation of OH chain length is a valuable tool in assessing the oxidative capacity of a given airmass and provides the quantitative rigor necessary to compare it to other airmasses.

4.4 Ozone production

Our comparison of ozone production to other studies focuses on magnitude and timing of ozone production. In terms of magnitude, we report similar values as those reported by Shirley et al. (2006) using RACM and by Lei et al. (2007) in a chemical transport study. Compared to other cities, we report much higher values of ozone production (Kleinman et al., 2005). The study by Ren et al. (2003), with under-predicted HO_2 concentrations in the model, observe a similar difference between $P(O_3)$ from measurements compared to the model as shown here in Fig. 8.

In the lower panel of Fig. 9, the shapes on the graph indicate the VOC_R and NO_x "coordinates" of $P(O_3)$ values reported in a 5-city study by Kleinman et al. (2005), with the range of $P(O_3)$ generally between 20–60 ppb h^{-1}. The higher ozone production rates reported for the MCMA are consistent with the higher VOC loadings and the high NO_x environment. Even though NO_x levels in the MCMA are up to an order of magnitude higher than other urban areas, the ozone production levels do not scale linearly because of the increased radical flux along loss routes for OH and RO_2 with NO_2 and NO, respectively. It is also worth noting that we consider our values for $P(O_3)$ as an under-estimate based on lower-than-expected RO_2 values. In other urban studies, as indicated by the dark and light gray shaded lines in Fig. 5B they note a RO_2-to-HO_2 ratio of roughly 1, whereas a HO_x-constrained calculation here indicates a much lower value (0.2); a RO_2-to-HO_2 value of 0.8, for instance, may result in ozone production levels about 40–50 ppb h^{-1} higher.

In terms of the timing, the measurements of OH, HO_2, NO, and NO_2 in the MCMA indicate a much different profile for ozone production than the model suggests. As shown in Fig. 8, the model clearly lacks the sharp peak around 08:00. Instead we observe a broad peak between 10:00–11:00, some 2 h after measurements suggest peak ozone production. Similarly, in the results presented by Shirley et al. (2006), peak ozone production is around 09:30, nearly 1.5 h later than expected. In the case presented by Lei et al. (2007) using a chemical transport model, they observe peak

ozone production around 12:30 (W. Lei, personal communication) more than 4 h later than expected by observations. In the PMTACS-NY study, measurements indicate peak ozone production around 09:00. In addition to a consistent under-prediction of ozone production by the model compared to measurements, models do not observe a distinct peak in ozone production in the early morning.

5 Conclusions

The near-explicit MCMv3.1 was constrained using an extensive suite of data from the MCMA-2003 field campaign to study radical cycling in the MCMA. We have constrained MCMv3.1 to calculate fluxes of RO_x radical initiation (Volkamer et al., 2007) routes and HO_x radical concentrations. The radical propagation fluxes and HO_x concentrations reported here indicate much higher photochemical activity than reported elsewhere in the literature, and are a reflection of the high VOC and NO_x loadings characteristic of the MCMA. We report excellent agreement between a lower-limit measured concentration and the modeled concentrations of OH using MCMv3.1, with a notable under-prediction around 06:00–07:00 (but still within measured and modeled uncertainties). Ongoing updates to the HO_x calibration may increase HO_x concentrations by up to a factor of 1.6 (W. H. Brune, personal communication); including this scaling factor will result in a significant under-prediction of both OH and HO_2. Notably, we already observe a significant under-prediction of HO_2 using the current calibration. This under-prediction of HO_x i.e., missing reactivity is most notable when NO_x concentrations are high (25–130 ppb). Despite a good correlation using a linear regression analysis for measured and modeled HO_x, we caution against this metric as it is weighted towards times when HO_x values are high and NO_x concentrations are low. The metric especially does not reflect photochemical activity (i.e., radical fluxes) and may simulate apparently good agreement between the model and measurements.

Two consistent ways to calculate chain length yield incompatible results if constrained for HO_x measurements. Assuming the HO_x measurements are correct, we

conclude that there are two possible explanations to resolve this inconsistency: 1) an additional RO_x radical source is needed, and 2) an additional HO_2 sink is required that does not form OH. Note, however, that both (1) and (2) are necessary in order for the chain length results to be consistent. Notably, the mechanism for the formation of HNO_3 via reaction between HO_2 and NO as reported by Butkovskaya et al. (2005) and Butkovskaya et al. (2007) is consistent with the second explanation listed above; however, only including the introduction of a HO_2 sink would increase missing reactivity in the model.

A significant measurement imbalance as indicated by calculations of OH production and loss affects the ability of our constrained mechanism to characterize accurately the oxidative capacity of the atmosphere. The reason(s) for the imbalance is unclear. Possible explanations for the imbalance include, but are not limited to, measurement uncertainties and micro-meteorological phenomena. The confirmation of the imbalance between observationally determined OH production and loss is no small task: It would require the co-location of multiple instruments capable of measuring HO_x concentrations in a polluted atmosphere, highly sensitive and highly time-resolved NO measurements (i.e., 100 ppt detection limit with seconds time resolution), and an extensive library of time-resolved VOC concentrations.

Control strategies for effective air quality management rely on the predictive capacity of models. The ozone production rates reported in this study are much higher than those reported elsewhere. Independent of the magnitude of ozone production, our results along with those from other studies indicate that models are often unable to predict the timing of RO_x-NO_x radical processing. Assuming that measured HO_2 radicals will propagate to form ozone, and a low RO_2-to-HO_2 ratio of 0.3, ozone production is under-predicted by factor of 2; this under-prediction will be higher with a ratio of RO_2-to-HO_2 closer to 1. The uncertainty due to "missing radicals" in models may appear reduced in urban airshed models that are optimized towards a specific target question (e.g., predicting ozone). However, the uncertainty inherent to the chemistry modules proves difficult to parameterize over a wide range of VOC and NO_x condi-

tions (Carter, 2004). For conditions typical for the VOC limited chemistry relevant in the MCMA the uncertainty in predicting ozone ranges between 10–40% (or several 10 ppb at peak ozone). This uncertainty is comparable to that from uncertain emission inventories and meteorology (Lei et al., 2007). Underestimating oxidant fields poses an additional modeling challenge with predicting the rapid formation of large amounts of secondary organic aerosol observed in urban air (Volkamer et al., 2006; Kleinman et al., 2007).

The uncertainty of chemistry modules has significant implications for predicting changes in ozone and aerosol concentrations as a result of varying VOC and NO_x inputs in future scenarios. There is a need for laboratory research that improves our understanding of RO_x radical cycling at high NO_x concentrations characteristic of polluted urban airsheds.

Acknowledgements. The authors would like to thank the entire MCMA-2003 team. In particular, we would like to thank W. H. Brune for detailed measurements of OH, HO_2 and OH-reactivity and helpful discussion related to these measurements. This work was supported by the National Science Foundation (ATM-0528227), the Department of Energy (DE-FG02-0563980), the Alliance for Global Sustainability (AGS), and the Comision Ambiental Metropolitana (CAM) of Mexico City. R. Volkamer acknowledges consecutive fellowships by the Henry and Camille Dreyfus Foundation and Alexander von Humboldt Foundation. P. Sheehy is grateful to J. I. Steinfeld.

References

Abram, J. P., Creasey, D. J., Heard, D. E., Lee, J. D., and Pilling, M. J.: Hydroxyl radical and ozone measurements in England during the solar eclipse of 11 August 1999, Geophys. Res. Lett., 27, 3437–3440, 2000. 5361

Axelsson, H., Eilard, A., Emanuelsson, A., Galle, B., Edner, H., Ragnarson, P., and Kloo, H.: Measurement of Aromatic-Hydrocarbons with the Doas Technique, Appl. Spectrosc., 49, 1254–1260, 1995. 5368

Bethel, H. L., Arey, J., and Atkinson, R.: Products of the OH radical-initiated reaction of 3-hexene-2,5-dione, Environ. Sci. Technol., 35, 4477–4480, 2001. 5365

Bloss, C., Wagner, V., Bonzanini, A., Jenkin, M. E., Wirtz, K., Martin-Reviejo, M., and Pilling, M. J.: Evaluation of detailed aromatic mechanisms (MCMv3 and MCMv3.1) against environmental chamber data, Atmos. Chem. Phys., 5, 623–639, 2005a. 5364, 5365, 5374, 5386

Bloss, C., Wagner, V., Jenkin, M. E., Volkamer, R., Bloss, W. J., Lee, J. D., Heard, D. E., Wirtz, K., Martin-Reviejo, M., Rea, G., Wenger, J. C., and Pilling, M. J.: Development of a detailed chemical mechanism (MCMv3.1) for the atmospheric oxidation of aromatic hydrocarbons, Atmos. Chem. Phys., 5, 641–664, 2005b. 5364, 5365, 5374, 5386

Butkovskaya, N., Kukui, A., and Le Bras, G.: HNO3 forming channel of the HO2+NOreaction as a function of pressure and temperature in the ranges of 72-600 torr and 223–323 K, J. Phys. Chem. A, 111, 9047–9053, 2007. 5392

Butkovskaya, N. I., Kukui, A., Pouvesle, N., and Le Bras, G.: Formation of nitric acid in the gas-phase HO2+NOreaction: Effects of temperature and water vapor, J. Phys. Chem. A, 109, 6509–6520, 2005. 5392

Carter, W. P. L.: Environmental Chamber Studies of Ozone Formation Potentials of Volatile Organic Compounds, Proceedings of the NATO Advanced Research Workshop "Environmental Simulation Chambers: Application to Atmospheric Chemical Processes", NATO Sciences Series, IV. Earth and Environmental Sciences, Kluwer Academic Publishers, Zakopane, Poland, 469 pp. , 2006. 5393

Curtis, A. and Sweetenham, W.: FACSIMILE/CEKMAT user's manual, Tech. Rep. AERE Rep-R12805, Her Majesty's Stationery Office, 1987. 5365

de Foy, B., Caetano, E., Magana, V., Zitacuaro, A., Cardenas, B., Retama, A., Molina, L., and Molina, M.: Mexico City basin wind circulation during the MCMA-2003 field campaign, Atmos. Chem. Phys., 5, 2267–2288, 2005, http://www.atmos-chem-phys.net/5/2267/2005/. 5370

Donahue, N. M., Robinson, A. L., Stanier, C. O., and Pandis, S. N.: Coupled partitioning, dilution, and chemical aging of semivolatile organics, Environ. Sci. Technol., 40, 2635–2643, 2006. 5384

Emmerson, K. M., Carslaw, N., Carpenter, L. J., Heard, D. E., Lee, J. D., and Pilling, M. J.: Urban atmospheric chemistry during the PUMA campaign 1: Comparison of modelled OH and HO_2 concentrations with measurements, J. Atmos. Chem., 52, 143–164, 2005. 5386

Emmerson, K. M., Carslaw, N., Carslaw, D. C., Lee, J. D., McFiggans, G., Bloss, W. J., Grave-

stock, T., Heard, D. E., Hopkins, J., Ingham, T., Pilling, M. J., Smith, S. C., Jacob, M., and Monks, P. S.: Free radical modelling studies during the UK TORCH Campaign in Summer 2003, Atmos. Chem. Phys., 7, 167–181, 2007, http://www.atmos-chem-phys.net/7/167/2007/. 5362, 5364, 5375, 5386, 5388

EPA: Hazardous Air Pollutants: EPA AirData Monitor Values Report, Tech. rep., US Environmental Protection Agency, http://www.epa.gov/air/data, 2004. 5400

Faloona, I., Tan, D., Brune, W. H., Jaegle, L., Jacob, D. J., Kondo, Y., Koike, M., Chatfield, R., Pueschel, R., Ferry, G., Sachse, G., Vay, S., Anderson, B., Hannon, J., and Fuelberg, H.: Observations of HOx and its relationship with NOx in the upper troposphere during SONEX, J. Geophys. Res.-Atmos., 105, 3771–3783, 2000. 5386

Folkins, I., Wennberg, P. O., Hanisco, T. F., Anderson, J. G., and Salawitch, R. J.: OH, HO_2, and NO in two biomass burning plumes: Sources of HOx and implications for ozone production, Geophys. Res. Lett., 24, 3185–3188, 1997. 5386

George, L. A., Hard, T. M., and O'Brien, R. J.: Measurement of free radicals OH and HO2 in Los Angeles smog, J. Geophys. Res.-Atmos., 104, 11 643–11 655, 1999. 5361, 5362

Harley, R. A., Hannigan, M. P., and Cass, G. R.: Respeciation of Organic Gas Emissions and the Detection of Excess Unburned Gasoline in the Atmosphere, Environ. Sci. Technol., 26, 2395–2408, 1992. 5367, 5368, 5400

Heard, D. E., Carpenter, L. J., Creasey, D. J., Hopkins, J. R., Lee, J. D., Lewis, A. C., Pilling, M. J., Seakins, P. W., Carslaw, N., and Emmerson, K. M.: High levels of the hydroxyl radical in the winter urban troposphere, Geophys. Res. Lett., 31, doi:10.1029/2004GL020544, 2004. 5361

Jenkin, M. E., Saunders, S. M., and Pilling, M. J.: The tropospheric degradation of volatile organic compounds: A protocol for mechanism development, Atmos. Environ., 31, 81–104, 1997. 5363, 5365

Kleinman, L., Springston, S., Daum, P., Lee, Y., Nunnermacker, L., Senum, G., Wang, J., Weinstein-Lloyd, J., Alexander, M., Hubbe, J., Ortega, J., Canagaratna, M., and Jayne, J.: The time evolution of aerosol composition over the Mexico City plateau, Atmos. Chem. Phys. Discuss., 7, 14 461–14 509, 2007. 5393

Kleinman, L. I., Daum, P. H., Lee, Y. N., Nunnermacker, L. J., Springston, S. R., Weinstein-Lloyd, J., and Rudolph, J.: Sensitivity of ozone production rate to ozone precursors, Geophys. Res. Lett., 28, 2903–2906, 2001. 5384

Kleinman, L. I., Daum, P. H., Lee, Y. N., Nunnermacker, L. J., Springston, S. R., Weinstein-

Lloyd, J., and Rudolph, J.: A comparative study of ozone production in five U.S. metropolitan areas, J. Geophys. Res.-Atmos., 110, D02301, doi:10.1029/2004JD005096, 2005. 5382, 5383, 5390, 5411

Lei, W., de Foy, B., Zavala, M., Volkamer, R., and Molina, L. T.: Characterizing ozone production in the Mexico City Metropolitan Area: a case study using a chemical transport model, Atmos. Chem. Phys., 7, 1347–1366, 2007, http://www.atmos-chem-phys.net/7/1347/2007/. 5390, 5393

Lurmann, F., Carter, W., and Coyner, L.: A surrogate species chemical reaction mechanism for urban-scale air quality simulation models, Tech. Rep. EPA/600/3-87/014, US Environmental Protection Agency, Research Triangle Park, NC, 1987. 5362

Martin, P., Tuazon, E. C., Aschmann, S. M., Arey, J., and Atkinson, R.: Formation and atmospheric reactions of 4,5-dihydro-2-methylfuran, J. Phys. Chem. A, 106, 11 492–11 501, 2002. 5365

Martinez, M., Harder, H., Brune, W., Di Carlo, P., Williams, E., Hereid, D., Jobson, T., Kuster, W., Roberts, J., Trainer, D., and Geyer, A.: The behavior of the hydroxyl and hydroperoxyl radicals during TexAQS2000. Abstract A12D-0174, in: AGU Fall Meeting, EOS Transactions, San Francisco CA, 2002. 5361

Martinez, M., Harder, H., Kovacs, T. A., Simpas, J. B., Bassis, J., Lesher, R., Brune, W. H., Frost, G. J., Williams, E. J., Stroud, C. A., Jobson, B. T., Roberts, J. M., Hall, S. R., Shetter, R. E., Wert, B., Fried, A., Alicke, B., Stutz, J., Young, V. L., White, A. B., and Zamora, R. J.: OH and HO2 concentrations, sources, and loss rates during the Southern Oxidants Study in Nashville, Tennessee, summer 1999, J. Geophys. Res.-Atmos., 108, 2003. 5361, 5363, 5375, 5386, 5388

Molina, L. T., Kolb, C. E., de Foy, B., Lamb, B. K., Brune, W. H., Jimenez, J. L., Ramos-Villegas, R., Sarmiento, J., Paramo-Figueroa, V. H., Cardenas, B., Gutierrez-Avedoy, V., and Molina, M. J.: Air quality in North America's most populous city - overview of the MCMA-2003 campaign, Atmos. Chem. Phys., 7, 2447–2473, 2007, http://www.atmos-chem-phys.net/7/2447/2007/. 5364

Olariu, R. I.: Atmospheric Oxidation of Selected Aromatic Hydrocarbons, Doctoral dissertation, Bergische Universitaet Gesamthochschule Wuppertal, 2001. 5365

Olariu, R. I., Barnes, I., Becker, K. H., and Klotz, B.: Rate coefficients for the gas-phase reaction of OH radicals with selected dihydroxybenzenes and benzoquinones, Int. J. Chem. Kinet., 32, 696–702, 2000. 5365

Platt, U., Alicke, B., Dubois, R., Geyer, A., Hofzumahaus, A., Holland, F., Martinez, M., Mihelcic, D., Klupfel, T., Lohrmann, B., Patz, W., Perner, D., Rohrer, F., Schafer, J., and Stutz, J.: Free radicals and fast photochemistry during BERLIOZ, J. Atmos. Chem., 42, 359–394, 2002. 5361, 5363, 5386

Ren, X. R., Harder, H., Martinez, M., Lesher, R. L., Oliger, A., Shirley, T., Adams, J., Simpas, J. B., and Brune, W. H.: HOx concentrations and OH reactivity observations in New York City during PMTACS-NY2001, Atmos. Environ., 37, 3627–3637, 2003. 5361, 5362, 5363, 5386, 5387, 5390

Robinson, A. L., Donahue, N. M., Shrivastava, M. K., Weitkamp, E. A., Sage, A. M., Grieshop, A. P., Lane, T. E., Pierce, J. R., and Pandis, S. N.: Rethinking organic aerosols: Semivolatile emissions and photochemical aging, Science, 315, 1259–1262, 2007. 5384, 5385, 5404

Salcedo, D., Onasch, T. B., Dzepina, K., Canagaratna, M. R., Zhang, Q., Huffman, J. A., DeCarlo, P. F., Jayne, J. T., Mortimer, P., Worsnop, D. R., Kolb, C. E., Johnson, K. S., Zuberi, B., Marr, L. C., Volkamer, R., Molina, L. T., Molina, M. J., Cardenas, B., Bernabe, R. M., Marquez, C., Gaffney, J. S., Marley, N. A., Laskin, A., Shutthanandan, V., Xie, Y., Brune, W., Lesher, R., Shirley, T., and Jimenez, J. L.: Characterization of ambient aerosols in Mexico City during the MCMA-2003 campaign with Aerosol Mass Spectrometry: results from the CENICA Supersite, Atmos. Chem. Phys., 6, 925–946, 2006, http://www.atmos-chem-phys.net/6/925/2006/. 5385

Saunders, S. M., Jenkin, M. E., Derwent, R. G., and Pilling, M. J.: Protocol for the development of the Master Chemical Mechanism, MCM v3 (Part A): tropospheric degradation of non-aromatic volatile organic compounds, Atmos. Chem. Phys., 3, 161–180, 2003, http://www.atmos-chem-phys.net/3/161/2003/. 5365

Seinfeld, J. H. and Pandis, S. N.: Atmospheric Chemistry and Physics : From Air Pollution to Climate Change, Wiley, New York, 1326 pp., 1998. 5375, 5381, 5388, 5389

Shirley, T. R., Brune, W. H., Ren, X., Mao, J., Lesher, R., Cardenas, B., Volkamer, R., Molina, L. T., Molina, M. J., Lamb, B., Velasco, E., Jobson, T., and Alexander, M.: Atmospheric oxidation in the Mexico City Metropolitan Area (MCMA) during April 2003, Atmos. Chem. Phys., 6, 2753–2765, 2006, http://www.atmos-chem-phys.net/6/2753/2006/. 5362, 5366, 5370, 5371, 5373, 5380, 5381, 5386, 5390, 5405, 5409

Stockwell, W. R., Kirchner, F., Kuhn, M., and Seefeld, S.: A new mechanism for regional atmospheric chemistry modeling, J. Geophys. Res.-Atmos., 102, 25 847–25 879, 1997. 5362

Stroud, C., Madronich, S., Atlas, E., Cantrell, C., Fried, A., Wert, B., Ridley, B., Eisele, F.,

Mauldin, L., Shetter, R., Lefer, B., Flocke, F., Weinheimer, A., Coffey, M., Heikes, B., Talbot, R., and Blake, D.: Photochemistry in the arctic free troposphere: Ozone budget and its dependence on nitrogen oxides and the production rate of free radicals, J. Atmos. Chem., 47, 107–138, 2004. 5375, 5388

Tan, D., Faloona, I., Simpas, J. B., Brune, W., Olson, J., Crawford, J., Avery, M., Sachse, G., Vay, S., Sandholm, S., Guan, H. W., Vaughn, T., Mastromarino, J., Heikes, B., Snow, J., Podolske, J., and Singh, H.: OH and HO2 in the tropical Pacific: Results from PEM-Tropics B, J. Geophys. Res.-Atmos., 106, 32 667–32 681, 2001. 5386

Velasco, E., Lamb, B., Westberg, H., Allwine, E., Sosa, G., Arriaga-Colina, J. L., Jobson, B. T., Alexander, M., Prazeller, P., Knighton, W. B., Rogers, T. M., Grutter, M., Herndon, S. C., Kolb, C. E., Zavala, M., de Foy, B., Volkamer, R., Molina, L. T., and Molina, M. J.: Distribution, magnitudes, reactivities, ratios and diurnal patterns of volatile organic compounds in the Valley of Mexico during the MCMA 2002 and 2003 field campaigns, Atmos. Chemi. Phys., 7, 329–353, 2007. 5367

Volkamer, R., Etzkorn, T., Geyer, A., and Platt, U.: Correction of the oxygen interference with UV spectroscopic (DOAS) measurements of monocyclic aromatic hydrocarbons in the atmosphere, Atmos. Environ., 32, 3731–3747, 1998. 5368

Volkamer, R., Platt, U., and Wirtz, K.: Primary and secondary glyoxal formation from aromatics: Experimental evidence for the bicycloalkyl-radical pathway from benzene, toluene, and p-xylene, J. Phys. Chem. A, 105, 7865–7874, 2001. 5365

Volkamer, R., Klotz, B., Barnes, I., Imamura, T., Wirtz, K., Washida, N., Becker, K. H., and Platt, U.: OH-initiated oxidation of benzene – Part I. Phenol formation under atmospheric conditions, Phys. Chem. Chem. Phys., 4, 1598–1610, 2002. 5365

Volkamer, R., Molina, L. T., Molina, M. J., Flores, E., Grutter, M., Galle, B., Mellqvist, J., Samuelsson, J., Knighton, B., and Jobson, B. T.: Open-path Emission Factors Derived from DOAS and FTIR Measurements in the Mexico City Metropolitan Area, American Geophysical Union, Fall Meeting Supplement, 85, Abstract A11A–0003, 2004. 5367

Volkamer, R., Molina, L., Molina, M., Shirley, T., and Brune, W. H.: DOAS measurement of glyoxal as an indicator for fast VOC chemistry in urban air, Geophys. Res. Lett., 32, L08806, doi:10.1029/2005GL022616, 2005. 5367, 5369

Volkamer, R., Jimenez, J. L., San Martini, F., Dzepina, K., Zhang, Q., Salcedo, D., Molina, L. T., Worsnop, D. R., and Molina, M. J.: Secondary organic aerosol formation from anthropogenic air pollution: Rapid and higher than expected, Geophys. Res. Lett., 33, 4,

doi:10.1029/2006GL026899, 2006. 5368, 5393

Volkamer, R., Sheehy, P., Molina, L., and Molina, M.: Oxidative capacity of the Mexico City atmosphere – Part 1: A radical source perspective, Atmos. Chem. Phys. Discuss., 7, 5365–5412, 2007, http://www.atmos-chem-phys-discuss.net/7/5365/2007/. 5361, 5364, 5365, 5368, 5369, 5371, 5378, 5380, 5384, 5386, 5389, 5391, 5405

Wagner, V., Jenkin, M. E., Saunders, S. M., Stanton, J., Wirtz, K., and Pilling, M. J.: Modelling of the photooxidation of toluene: conceptual ideas for validating detailed mechanisms, Atmos. Chem. Phys., 3, 89–106, 2003, http://www.atmos-chem-phys.net/3/89/2003/. 5375, 5376, 5377

Wall, K. J., Schiller, C. L., and Harris, G. W.: Measurements of the HONO photodissociation constant, J. Atmos. Chem., 55, 31–54, 2006. 5369

Table 1. VOC constraints used for box modeling based on measurements from MCMA-2003. The input for each species is determined by either **(A)** continuous measurement, **(B)** scaling to a continuous measurement via speciation as determined by co-located canister sampling, or **(C)** scaled to a continuous measurement via emission factors taken from Harley et al. (1992) and EPA.

alkanes		alkenes		aromatics		oxygenates (ctd)	
species	SF x10^{-2}	species	SF x10^{-2}	species	SF x10^{-2}	species	SF x10^{-2}
methane	FTIR	ethene	80 [C]	benzene	DOAS	methanol	PTRMS
ethane	2.18 [A]	propene	44 [C]	toluene	DOAS	ethanol	15 [H]
propane	42.6 [A]	2-methylpropene	31 [C]	m-xylene	DOAS	1-propanol,2-propanol	5
i-butane	7.40 [A]	c-2-butene	4.5 [C]	p-xylene	DOAS	1-butanol,2-butanol	2 [H]
n-butane	19.7 [A]	t-2-butene	5.0 [C]	styrene	DOAS	2-methyl-1(2)-propanol	2 [H]
i-pentane	8.37 [A]	1-pentene	5.9 [C]	benzaldehyde	DOAS	ethylene glycol	25 [H]
n-pentane	3.69 [A]	c-2-pentene	2.8 [C]	ethyl benzene	62 [F]	propylene glycol	10 [H]
n-hexane	1.98 [A]	t-2-pentene	5.0 [C]	n-propyl benzene	16 [F]	2-methoxy ethanol	2 [H]
2-methylpentane	2.77 [A]	2-methyl-1-butene	12 [C]	i-propyl benzene	22 [F]	2-ethoxy ethanol	2 [H]
3-methylpentane	1.95 [A]	2-methyl-2-butene	8.5 [C]	o-xylene	53 [E]	1-methoxy 2-propanol	2 [H]
2,2-dimethylbutane	0.97 [A]	1,3-butadiene	4.8 [C]	1,2,4-trimethylbenzene	55 [E]	2-butoxy ethanol	2 [H]
2,3-dimethylbutane	0.64 [A]	isoprene	3.9 [C]	1,3,5-trimethylbenzene	19 [E]	1-butoxy 2-propanol	2 [H]
n-heptane	0.64 [A]	1-butene	15 [D]	1,2,3-trimethylbenzene	14 [E]	acetone	PTRMS
2-methylhexane	0.80 [A]	3-methyl-1-butene	5.9 [D]	o-ethyl toluene	14 [E]	methyl ethyl ketone	PTRMS
3-methylhexane	1.10 [A]	1-hexene	2.1 [D]	p-ethyl toluene	30 [E]	acetic acid	PTRMS
n-octane	0.26 [A]	c-2-hexene	2.1 [D]	m-ethyl toluene	14 [E]	methyl i-butyl ketone	13 [I]
n-nonane	0.22 [A]	t-2-hexene	3.8 [D]	**oxygenates**		ethyl acetate	0.6 [E]
n-decane	0.27 [A]	2,3-dimethyl-2-butene	2.1 [D]	formaldehyde (HCHO)	DOAS	n-propyl + i-propyl acetate	0.15 [E]
cyclohexane	0.31 [A]	acetylene	1.9 [E]	acetaldehyde	PTRMS	n-butyl acetate	0.21 [E]
n-undecane	1.6 [B]			propanal	4.5 [G]	methyl t-butyl ether	1.1 [E]
n-dodecane	0.32 [B]						

[A]-scaled to FTIR(C−H) based on canister speciation
[B]-scaled to FTIR(C−H) based on emission factors
[C]-continuous FOS signal scaled based on canister speciation
[D]-scaled to FOS signal based on emissions factors
[E]-scaled to DOAS-benzene based on canister speciation
[F]-scaled to mono-substituted benzene DOAS profile based on canister speciation
[G]-scaled to DOAS-HCHO based on emissions factors
[H]-scaled to PTRMS-CH_3OH based on emission factors
[I]-scaled to PTRMS-MEK based on emission factors

Table 2. Average reaction rates for RO_x radical pathways on individual days (in April) during MCMA-2003 from 07–13, as determined by a HO_x-unconstrained (left) and HO_x-constrained (right) model in units of 10^5 molec. cm^{-3} s^{-1}. Averaged values for n(OH), $P(O_3)$, VOC-reac., NO, $J(NO_2)$, and daily maxima of O_3, boundary layer height, CO are also shown to aid in the comparison of daily variations.

		9		10		11		12		13		14		15		16		17	
I1	OH initiation	139	140	284	284	232	233	193	193	252	253	147	147	323	324	244	243	265	266
T1	OH termination	232	216	370	371	273	385	211	241	247	219	198	206	365	286	330	376	354	317
I2	RO_2 initiation	82	80	171	172	120	178	108	129	144	142	89	93	166	150	152	167	153	147
T2	RO_2 termination	60	55	269	268	190	258	186	222	250	216	133	150	293	217	220	251	216	200
I3	RO initiation	6	4	8	8	13	15	5	6	8	7	4	4	9	8	9	10	9	8
T3	RO termination	20	18	33	33	22	34	20	26	24	24	18	18	37	32	33	38	31	29
I4	HO_2 initiation	102	100	262	263	181	289	150	173	195	193	134	137	260	242	234	249	228	221
T4	HO_2 termination	1	1	13	11	11	14	17	23	26	25	7	13	15	12	16	19	12	15
P1	$OH \rightarrow RO_2$	843	686	1445	1445	1345	1770	855	981	1284	1133	735	776	1503	1157	1265	1461	1308	1160
P2	$RO_2 \rightarrow RO$	755	620	1148	1152	1216	1585	690	788	1073	972	588	606	1170	938	1034	1191	1126	998
	via NO	505	432	840	835	855	1081	517	571	802	703	428	426	855	661	754	847	812	695
	via RO_2	236	176	293	294	376	475	173	202	271	250	160	169	315	259	280	321	313	285
P-2	$RO \rightarrow RO_2$	139	102	200	200	267	332	122	142	185	167	101	107	220	175	196	225	206	186
P3	$RO \rightarrow HO_2$	574	476	877	880	903	1190	525	600	817	741	450	463	886	709	777	896	854	756
P4	$HO_2 \rightarrow OH$	1047	2628	1750	2844	1553	5424	993	1735	1460	2322	893	1740	1796	2318	3691	3491	1587	2889
P5	$OH \rightarrow HO_2$	105	78	205	204	156	231	113	132	171	149	101	112	237	183	179	204	180	166
	chain length	2.8	9.2	2.6	5.0	3.0	8.8	2.5	4.2	2.8‘	4.2	2.6	4.9	2.6	3.9	2.6	5.9	2.6	4.5
	$P(O_3)$ (ppb/hr)	27.2	54.0	42.3	62.5	40.0	115.1	24.1	38.5	37.3	52.2	21.2	36.8	42.7	50.5	37.3	78.8	39.0	61.9
	O_{3max} (ppb)	130		146		78		150		109		144		156		156		115	
	VOC-reactivity (s^{-1})	49		50		67		37		43		28		35		52		42	
	NO (ppb)	37		36		54		15		16		17		17		37		26	
	$J(NO_2)$ ($x10^{-3}$ s^{-1})	2.7		5.5		5.4		6.7		6.5		5.8		6.1		6.0		6.3	
	PBL (km)	1.9		1.9		2.3		–		3.3		2.9		3.5		3.5		3.3	
	CO_{max} (ppm)	4.2		5.2		8.5		4.2		4.0		2.8		2.5		4.7		3.4	
	meteorology	cold surge		cold surge		cold surge		O3-North		O3-North		O3-South		O3-South		O3-South		O3-South	

ACPD
8, 5359–5412, 2008

Table 2. Continued.

		18		19		20		21		22		23		24		25		26	
I1	OH initiation	84	84	211	212	222	223	262	263	252	254	278	278	205	206	211	212	183	183
T1	OH termination	79	52	226	200	216	191	253	243	221	143	298	250	161	139	278	286	233	216
I2	RO_2 initiation	54	48	149	146	144	142	156	155	159	132	210	199	98	99	145	155	153	156
T2	RO_2 termination	79	62	238	203	240	195	272	236	302	182	343	272	187	131	221	203	227	196
I3	RO initiation	2	1	6	5	7	6	7	6	7	4	9	7	4	3	7	7	7	6
T3	RO termination	10	7	25	23	23	22	29	29	27	20	40	37	19	18	30	33	29	30
I4	HO_2 initiation	81	73	215	211	213	210	237	235	231	200	319	306	156	153	242	252	245	248
T4	HO_2 termination	29	28	36	35	48	33	52	35	46	20	68	41	51	31	31	29	51	39
P1	$OH \rightarrow RO_2$	522	336	1255	1101	1231	1062	1272	1168	1337	840	1575	1310	844	661	1164	1160	1066	972
P2	$RO_2 \rightarrow RO$	419	276	1027	928	1011	913	1009	959	1061	717	1256	1096	669	573	963	999	881	840
	via NO	273	175	744	648	727	634	744	685	766	495	923	778	475	394	710	717	642	592
	via RO_2	146	96	283	262	284	262	265	255	295	209	333	297	194	168	253	263	239	232
P-2	$RO \rightarrow RO_2$	72	49	168	150	178	159	175	165	181	120	223	191	122	100	172	173	164	152
P3	$RO \rightarrow HO_2$	330	215	791	715	771	698	771	733	815	550	962	840	511	439	730	759	666	637
P4	$HO_2 \rightarrow OH$	620	791	1476	1940	1434	1954	1490	2257	1517	1177	1864	2979	970	1768	1426	3719	1303	2638
P5	$OH \rightarrow HO_2$	96	62	195	170	198	167	215	193	199	126	255	208	161	112	185	173	177	154
	chain length	3.1	4.3	3.0	4.4	2.8	4.1	2.7	5.4	2.9	3.0	2.8	5.4	2.5	5.2	2.7	6.9	2.6	5.7
	$P(O_3)$ (ppb/hr)	15	17	37	45	36	45	37	51	38	29	47	66	24	38	35	78	32	57
	O_{3max} (ppb)	77		135		117		136		147		58		132		122		121	
	VOC-reactivity (s^{-1})	13		35		32		36		35		49		29		45		38	
	NO (ppb)	4		13		12		20		13		28		20		28		16	
	$J(NO_2)$ ($x10^{-3}$ s^{-1})	6.2		6.0		6.2		5.8		5.8		6.8		6.8		6.8		6.8	
	PBL (km)	3.1		1.5		2.5		2.9		1.5		–		3.5		3.5		3.0	
	CO_{max} (ppm)	1.6		2.8		2.4		3.9		1.9		4.6		3.8		5.8		4.3	
	meteorology	O3-North		cold surge		cold surge		cold surge		cold surge		O3-North		O3-North		O3-North		O3-North	

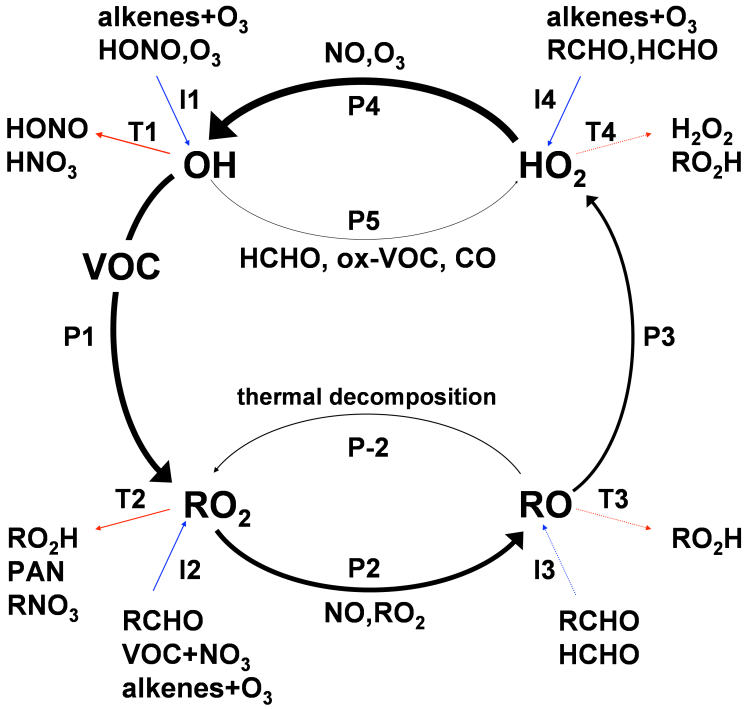

Fig. 1. The schematic of RO_x cycling in MCMA is shown. Only the predominant species involved in radical sources, sinks, and cycling are shown. Radical pathways are labeled as initiation (I), propagation (P), or termination (T), and assigned a number for cross-referencing in Table 1. The thickness of each arrow corresponds to the magnitude of the radical pathway, as determined in the HO_x-unconstrained scenario.

ACPD
8, 5359–5412, 2008

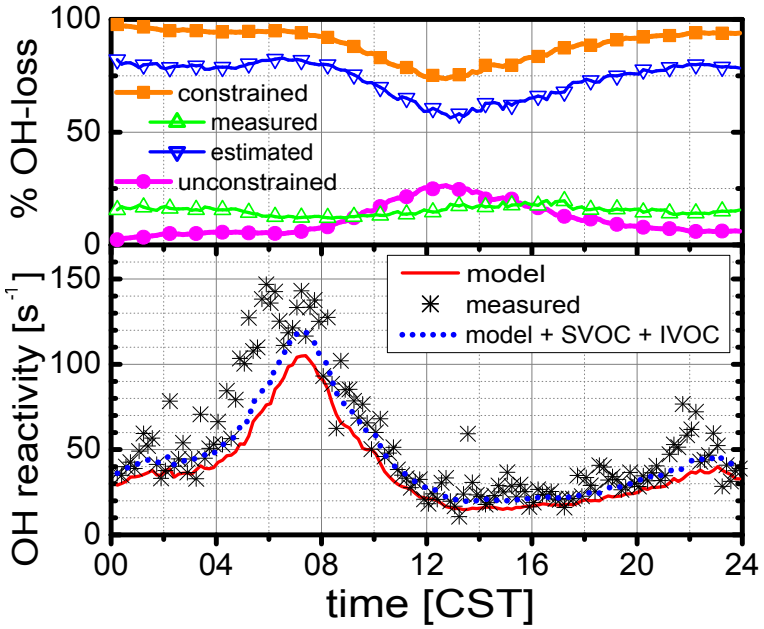

Fig. 2. The bottom panel shows the median measured (stars) and modeled (red solid line) OH loss; we also include a plot of modeled OH loss augmented with an estimated OH loss due to primary organic aerosol (POA) vapors (SVOC+IVOC) as parameterized by Robinson et al. (2007). Note the under-estimation of OH loss by the model between 05:00–07:00. The profile of OH loss in the model is separated into constrained parameters (square) and unconstrained parameters (circle). The constrained parameters are further distinguished as parameters constrained by measurements (triangle up) and those that were estimated (triangle down) based on emissions information in the literature. Constrained parameters account for some 75–98% of total modeled OH loss throughout the day.

ACPD
8, 5359–5412, 2008

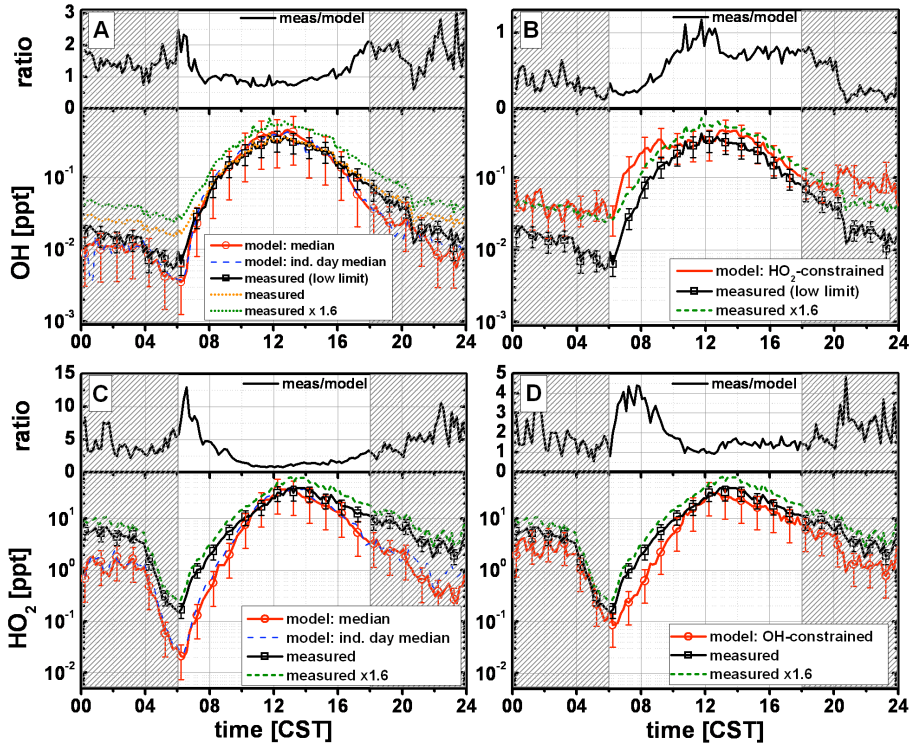

Fig. 3. Measured (circle) and modeled (square) diurnal concentrations of HO_x are shown for each of the three cases in steady-state: **(A)** OH, HO_x-unconstrained, **(B)** OH, HO_2-constrained, **(C)** HO_2, HO_x-unconstrained, and **(D)** HO_2, OH-constrained. In the upper panel of each graph, the measured-to-modeled ratios are also shown. Note that for the top panels of OH, A and B, "measured" refers to values reported by Shirley et al. (2006), "measured, lower limit" includes a 0.01 ppt offset subtracted from the measured values as discussed in the text and in Volkamer et al. (2007), and "measured x1.6" accounts for the potential adjustment to the reported measurements (W. H. Brune, personal communication).

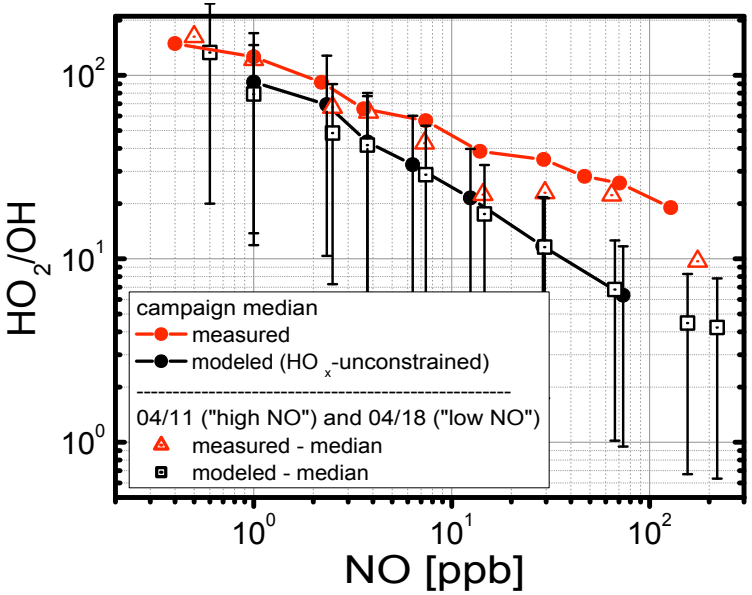

Fig. 4. The HO_2-to-OH ratio as a function of NO. The predicted values from the model on a campaign averaged basis are shown as the black line with circles, whereas the median measured values from the entire campaign are shown as a red line with circles. The symbols represent the HO_x ratio with respect to NO on individual days: measurements (red triangle) and modeled results (black square). Note that the lines are not a fit through the symbols.

ACPD
8, 5359–5412, 2008

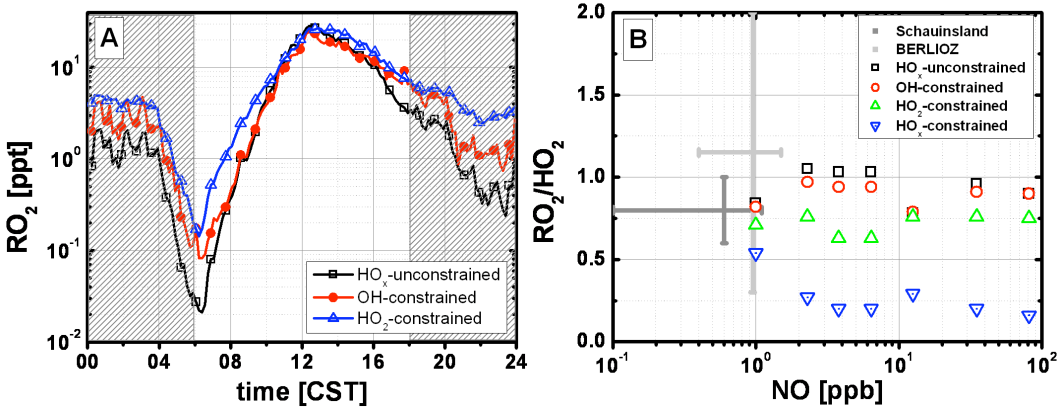

Fig. 5. Predicted RO_2 concentrations **(A)** and the ratio of RO_2 to HO_2 vs NO **(B)** for different modeling scenarios: HO_x-unconstrained (black squares), OH-constrained (red circles), and HO_2-constrained (blue triangle-up), and HO_x-constrained (green triangle-down). The RO_2 concentration demonstrates an expected near-linear dependence on OH concentration. The steady-state models similarly predict RO_2/HO_2 ratios ~1 at concentrations of NO ranging from 1–100+ ppb; however, the HO_x-constrained case predicts a much lower ratio, particularly at high NO (>7 ppb).

ACPD
8, 5359–5412, 2008

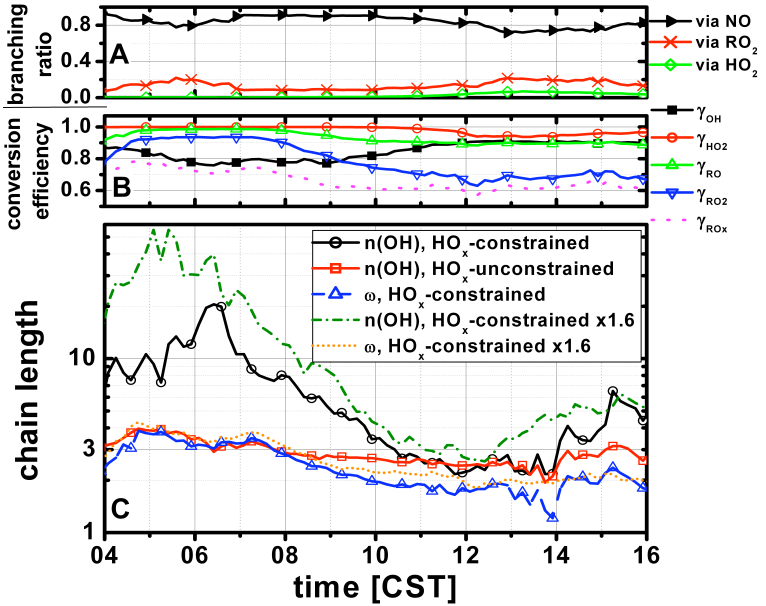

Fig. 6. Chain length values as calculated for the HO_x-constrained (black line) and HO_x-unconstrained (red dotted line) scenarios are shown in the lower panel **(C)**, along with the wheel parameter as described in Eqs. (1) and (12) (blue dashed line). The chain lengths (n(OH)) differ by as much as a factor of 7 (around 06:40), coincident with missing HO_x reactivity. The middle panel **(B)** shows the conversion factors, γ, for the HO_x-constrained case, and the product of them (dotted magenta line). The product of the conversion factors is linked to ω the wheel parameter. The upper panel **(A)** breaks down the branching ratios of RO_2 radical reaction pathways via NO, RO_2, and HO_2; this is to demonstrate that the afternoon chemistry is not NO_x-limited, but is still very much driven by NO_x and much less by organic peroxyl radicals formed as products of secondary oxidation.

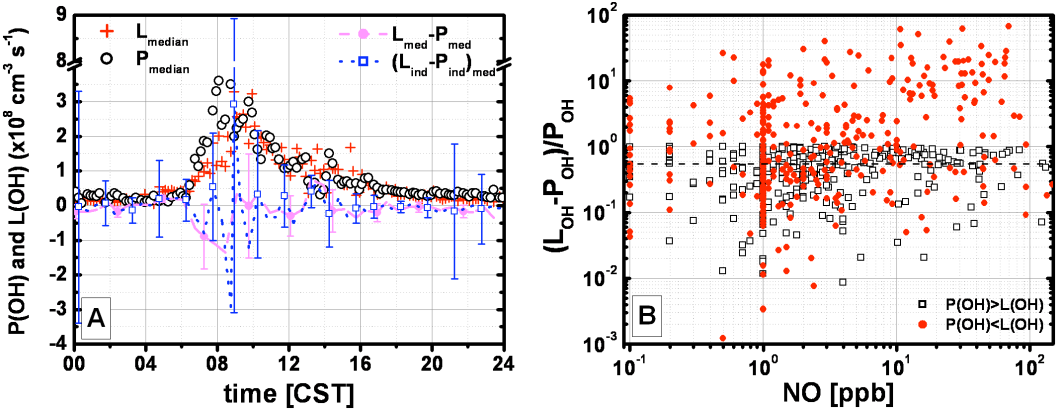

Fig. 7. (A) Median OH production (open black circles) and loss (red plusses) are plotted against the difference between them with a 2σ experimental uncertainty, as replicated from Shirley et al. (2006) (closed magenta circles, dashed line). The median difference between individual experimentally determined P(OH) and L(OH) terms is shown (blue open square, dotted line) with a 2σ standard deviation. (Note the break in the y-scale between 4–7×10^8 cm^{-3} s^{-1}; the error bars extend equally as far in the negative direction but are not shown). **(B)** The difference in OH production and loss is shown in relative terms by dividing by production (and when values are negative, the absolute value was used). The values are separated by P(OH)>L(OH) (black squares) and P(OH)<L(OH) (red circles). In principle, the difference should be 0. The dotted line represents an inferred experimental uncertainty, meaning that all points above this line fall outside a 2σ experimental uncertainty and represent an imbalance in the measurements.

ACPD
8, 5359–5412, 2008

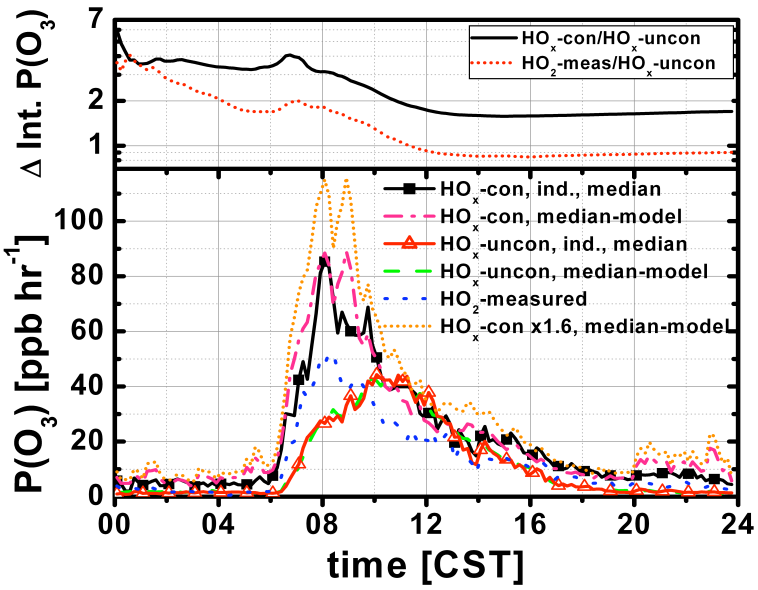

Fig. 8. The median diurnal profile for ozone production for individual day modeling is shown for the HO_x-constrained (black, squares) and HO_x-unconstrained (red, triangles), as well as for the median-model runs for HO_x-constrained (magenta, dash-dot) and HO_x-unconstrained (green, dash). Finally, $P(O_3)$ as calculated using only measured HO_2 is shown as the blue dotted line. The top panel results from dividing the integral of the median $P(O_3)_{HOx\text{-}con}$ by the median $P(O_3)_{HOx\text{-}uncon}$ (black line) and median $P(O_3)_{HO_2\text{-}con}$ by the median $P(O_3)_{HOx\text{-}uncon}$ (red dotted line).

ACPD
8, 5359–5412, 2008

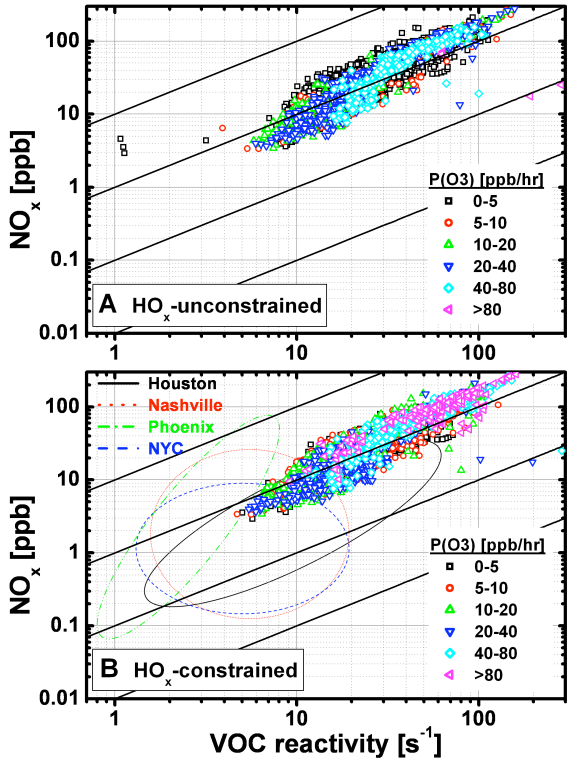

Fig. 9. Ozone production rates shown are shown as a function of VOC_R and NO_x in the HO_x-unconstrained **(A)** and HO_x-constrained cases **(B)**. Note the increased prevalence of higher $P(O_3)$ values in panel B (80+ppb hr^{-1}), as represented by the magenta left-triangles. Panel **(B)** also shows traces of ozone production rates as determined for other cities (Kleinman et al., 2005): Houston (black, solid line), Nashville (red, dotted line), Phoenix (green, dash-dot line), and New York City (blue, dashed line). The diagonal isolines represent constant VOC_R/NO_x ratios.

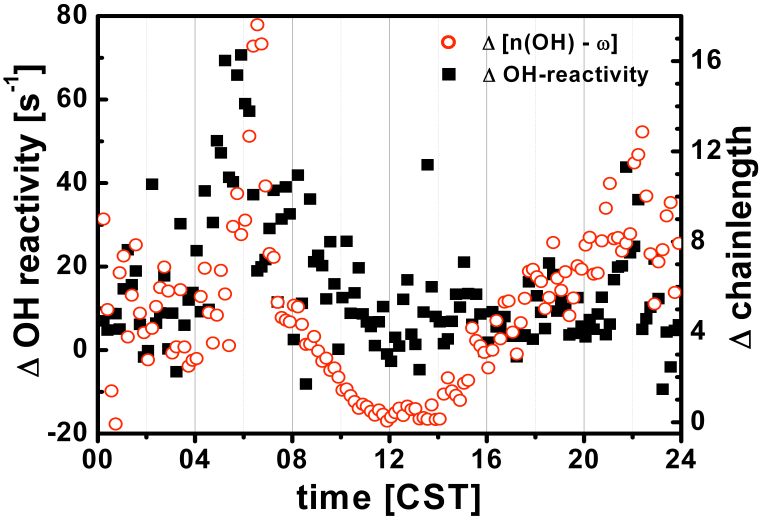

Fig. 10. The difference between measured OH reactivity and modeled OH reactivity (black squares) is plotted against the difference between the HO_x-constrained chain length parameters, n(OH) and ω (red circles). We observe a strong correlation between the missing reactivity observed in the early morning, around 06:00, and the difference in chain length parameters.

ACPD
8, 5359–5412, 2008